Hearing Research 392 (2020) 107973

Contents lists available at ScienceDirect

Hearing Research

journal homepage: www.elsevier.com/locate/heares

Research Paper

Morphological and molecular correlates of altered hearing sensitivity in the genetically audiogenic seizure-prone hamster GASH/Sal

David Sánchez-Benito [a, b], Miguel A. Hyppolito [c], Antonio J. Alvarez-Morujo [a, b, d], Dolores E. López [a, b, e], Ricardo Gómez-Nieto [a, b, e, *]

[a] Institute of Neuroscience of Castilla y León (INCYL), University of Salamanca, Salamanca, Spain
[b] Institute of Biomedical Research of Salamanca (IBSAL), University of Salamanca, Salamanca, Spain
[c] Laboratory of Neurobiology of Hearing, Department of Ophthalmology, Otorhinolaryngology, Head and Neck Surgery, Ribeirão Preto Medical School, University of São Paulo, São Paulo, Brazil
[d] Department of Human Anatomy and Histology, Faculty of Medicine, University of Salamanca, Salamanca, Spain
[e] Department of Cell Biology and Pathology, Faculty of Medicine, University of Salamanca, Salamanca, Spain

ARTICLE INFO

Article history:
Received 8 January 2020
Received in revised form
30 March 2020
Accepted 7 April 2020
Available online 26 April 2020

Keywords:
Animal models of epilepsy
Cochlear neuropathy
Cochlear nucleus
VGLUT
Audiogenic seizures
Spiral ganglion neurons

ABSTRACT

Rodent models of audiogenic seizures, in which seizures are precipitated by an abnormal response of the brain to auditory stimuli, are crucial to investigate the neural bases underlying ictogenesis. Despite significant advances in understanding seizure generation in the inferior colliculus, namely the epileptogenic nucleus, little is known about the contribution of lower auditory stations to the seizure-prone network. Here, we examined the cochlea and cochlear nucleus of the genetic audiogenic seizure hamster from Salamanca (GASH/Sal), a model of reflex epilepsy that exhibits generalized tonic–clonic seizures in response to loud sound. GASH/Sal animals under seizure-free conditions were compared with matched control hamsters in a multi-technical approach that includes auditory brainstem responses (ABR) testing, histology, scanning electron microscopy analysis, immunohistochemistry, quantitative morphometry and gene expression analysis (RT-qPCR). The cochlear histopathology of the GASH/Sal showed preservation of the sensory hair cells, but a significant loss of spiral ganglion neurons and mild atrophy of the stria vascularis. At the electron microscopy level, the reticular lamina exhibited disarray of stereociliary tufts with blebs, loss or elongated stereocilia as well as non-parallel rows of outer hair cells due to protrusions of Deiters' cells. At the molecular level, the abnormal gene expression patterns of *prestin, cadherin 23, protocadherin 15, vesicular glutamate transporters 1 (Vglut1) and -2 (Vglut2)* indicated that the hair-cell mechanotransduction and cochlear amplification were markedly altered. These were manifestations of a cochlear neuropathy that correlated to ABR waveform I alterations and elevated auditory thresholds. In the cochlear nucleus, the distribution of VGLUT2-immunolabeled puncta was differently affected in each subdivision, showing significant increases in magnocellular regions of the ventral cochlear nucleus and drastic reductions in the granule cell domain. This modified inputs lead to disruption of *Vglut1* and *Vglut2* gene expression in the cochlear nucleus. In sum, our study provides insight into the morphological and molecular traits associated with audiogenic seizure susceptibility in the GASH/Sal, suggesting an upward spread of abnormal glutamatergic transmission throughout the primary acoustic pathway to the epileptogenic region.

1. Introduction

Epilepsy research has made significant progress thanks to a wide range of animal models that, to a greater or lesser extent, mimics the variety of clinical, electrophysiological, and behavioral manifestations that comprise epilepsy syndromes. A comparative approach using animal models of epilepsies uncovered many of the deficits associated with the epileptic brain, providing unique insights into

* Corresponding author. Institute of Neuroscience of Castilla y León (INCyL), Laboratory of Audiomotor Disorders, C/ Pintor Fernando Gallego, 1, 37007, Salamanca, Spain.
E-mail address: richard@usal.es (R. Gómez-Nieto).

https://doi.org/10.1016/j.heares.2020.107973

aspects of ictogenesis (Grone and Baraban, 2015), and leading to discovery of anti-seizure treatment strategies (Loscher, 2011). Audiogenic seizure (AGS) is a type of generalized clonic or tonic-clonic convulsive muscle contractions caused by excessive or abnormal neuronal firing in response to intense sound stimulation. AGS is frequent in rodents, in which susceptibility can occur genetically or be induced by a large variety of experimental treatments such as priming procedures (Ross and Coleman, 2000; Garcia-Cairasco, 2002). Using acoustic priming, several rodent strains not initially AGS-susceptible become seizure prone by exposure to an acoustic insult during a critical period of postnatal development (e.g. Pierson and Snyder-Keller, 1994). For genetically prone strains of rodents, the priming procedure is not required and seizures are elicited by high-intensity acoustic stimulation just a few weeks after birth (Ross and Coleman, 2000). In contrast to traditional models of epilepsy induced by chemical or electrical means or primed models, the AGS rodents of genetic origin offer several advantages. Firstly, the AGS susceptibility is inherited and does not require any experimental procedure to become susceptible, avoiding thus incompatibilities with experimental designs that require anti-seizure drugs administration or the possibility of chemically or electrically modulating seizures (Kandratavicius et al., 2014). In addition, the innate occurring seizures can be elicited at will by an investigator, as the specific trigger is a sound. A further advantage lies in the substantial characterization of behavioral, cellular, and molecular alterations available of genetically AGS models that potentiates their usefulness in elucidating mechanisms and neuronal substrates underlying the seizure genesis and propagation (Ross and Coleman, 2000; Kandratavicius et al., 2014). Examples of genetically seizure-prone strains of rodents include mainly rats and mice such as the genetically epilepsy-prone rat (GEPR; Reigel et al., 1986), the Wistar audiogenic rat (WAR; Doretto et al., 2003), the DBA/2 mouse (De Sarro et al., 2017), the Black Swiss mouse (BLSW, Charizopoulou et al., 2011) and the Frings mouse (Skradski et al., 2001). The only available hamster strain that exhibits susceptibility to sound-induced seizures is the genetic audiogenic seizure hamster from Salamanca (GASH/Sal) that presents an autosomal recessive inheritance pattern (Muñoz et al., 2017). The GASH/Sal has recently gathered attention as a model for sensory-evoked reflex seizures precisely for the amount of interesting data related to the neuroethological (Barrera-Bailón et al., 2013, 2017), electrophysiological (Carballosa-Gonzalez et al., 2013), neurochemical (Prieto-Martín et al., 2017), molecular (López-López et al., 2017; Díaz-Casado et al., 2020) and morphological (Sánchez-Benito et al., 2017) substrates underlying AGS. Nearly 100% of the GASH/Sal strain, from 2 to 4 months of age at which susceptibility reached its maximum, undergoes generalized tonic–clonic seizures that are characterized by a short latency period after loud acoustic stimulation, followed by phases of wild running, convulsions, and stupor, with origin in the brainstem (Muñoz et al., 2017). Anticonvulsant drugs are very effective in suppressing sound-induced seizures in the GASH/Sal (Barrera-Bailón et al., 2013, 2017; Werner and Coveñas, 2017), and hence clarification of molecular and neuronal mechanisms leading to susceptibility of AGS could have important implications for the use of the GASH/Sal model in development of new anti-seizure agents. Activation of auditory pathways is required for seizure development in all AGS models, and many studies pointed out the inferior colliculus, a critical integration center in the auditory midbrain pathway, as the epileptogenic focus (reviewed in Garcia-Cairasco, 2002). This implies that defects in lower auditory structures might be common among AGS models, thereby causing alterations of bottom-up auditory inputs to the inferior colliculus. In this regard, cochlear abnormalities have been identified in the GEPR model (Penny et al., 1983), and electrolytic destruction of the ventral cochlear nucleus was reported to cause a blockade of audiogenic convulsions in rats (Browning, 1986). In the GASH/Sal, auditory-evoked brainstem responses (ABR) and distortion-product of otoacoustic emissions analyses revealed an altered hearing sensitivity with increased ABR thresholds and absence of otoacoustic emissions in a wide range of frequencies (Muñoz et al., 2017; Sánchez-Benito et al., 2017). Consequently, such hearing impairments were correlated with morphological alterations in the olivocochlear efferent system that reflexively modulates the sensitivity of receptor mechanisms operating in the cochlear hair cells (Sánchez-Benito et al., 2017). In the current study, we used histology, scanning electron microscopy analysis and quantitative morphometry to examine in detail the major sites of the cochlear pathology in the GASH/Sal. These elements include: 1) the two anatomically and functionally distinct types of mechanosensitive receptor cells within the organ of Corti, the inner and outer hair cells (IHCs and OHCs, respectively); 2) the spiral ganglion neurons (SGNs) that relay auditory inputs from the cochlear hair cells to the cochlear nucleus; and 3) the stria vascularis (SV) that is essential for transporting oxygen and nutrients into the cochlea. We further sought to determine the possible molecular defects associated to the cochlear histopathology of the GASH/Sal. By using the reverse transcription-quantitative polymerase chain reaction (RT-qPCR), we analyzed mRNA expression levels of key cochlear genes such as *prestin* (*Slc26a5*), *cadherin 23* (*Cdh23*), and *protocadherin 15* (*Pcdh15*) that are involved in the function and integrity of the sensory hair cells (Kazmierczak et al., 2007; Xia et al., 2013). Given that cochlear neuropathy is associated with damage at the cochlear synapse without loss of sensory hair cells, and is often accompanied by adaptive responses and hyperexcitability in auditory brainstem nuclei (Salvi et al., 2000; Rachel et al., 2002; Mulders et al., 2011; Liberman and Kujawa, 2017), we also determine whether the cochlea and cochlear nucleus of the GASH/Sal exhibit altered gene expression of vesicular glutamate transporters 1 (*Vglut1*) and −2 (*Vglut2*). VGLUT1 and -2, encoded by two separate genes, are primarily localized in axon terminals and define two distinct classes of excitatory synapsis with a non-overlapping distribution (Takamori et al., 2001; Fremeau et al., 2001). In the cochlear nucleus, these two VGLUT isoforms have been used to differentiate glutamate signaling inputs as auditory nerve terminals preferentially colabeled with VGLUT1 and somatosensory terminals with VGLUT2 (Furness and Lawton, 2003; Zhou et al., 2007; Gómez-Nieto and Rubio, 2009). In addition, several studies showed correlations between changes in VGLUT2-immunoreactivity and disorders characterized by hyperexcitability such as epilepsy (Wallen-Mackenzie et al., 2010) and tinnitus (Heeringa et al., 2018). Thus, we analyzed the distribution of VGLUT2 axon terminals in the cochlear nucleus subdivisions of the GASH/Sal model. The overall goal of this study was to present a comprehensive picture of a cochlear neuropathy that may generate hyperexcitability in central auditory pathways and therefore bring about an upstream seizure-prone circuitry. In particular, we show a link of functional, molecular and morphological correlations between the peripheral pathologies and glutamatergic imbalance in the cochlear nucleus that might underlie the innate audiogenic seizure susceptibility of the GASH/Sal model. Since the outcomes of the present study were based on the comparisons with age-matched wild-type Syrian hamsters, our study also provides valuable information of the auditory peripheral system and the cochlear nucleus of the *Mesocricetus auratus*.

2. Material and methods

2.1. Experimental animals

In total, 15 control hamsters (*Mesocricetus auratus*) from Janvier Labs (Le Genest-Saint-Isle, France) and 14 hamsters of the GASH/Sal strain from the animal's facility of the University of Salamanca

(Salamanca, Spain), with 4 months of age, were used in this study. We selected animals of that age because the GASH/Sal exhibits the maximum susceptibility to seizures from 2 to 4 months of age (Muñoz et al., 2017). All the GASH/Sal were males and naïve without receiving any acoustic stimulation to trigger audiogenic seizures. The experiments were conducted in compliance with the guidelines for the use and care of laboratory animals of the European Communities Council Directive (2010/63/EU), the current Spanish legislation (RD 1201/05), and with those established by the Institutional Bioethics Committee (approval number 300). All efforts were made to minimize the number of animals and their suffering. The animals were maintained under normal conditions of lighting (12 h light/dark cycle) and constant temperature with *ad libitum* access to food and water.

2.2. ABR recordings and analysis

The ABR testing followed a similar procedure previously described by Colmenárez-Raga et al. (2019). 4 control and 4 GASH/Sal hamsters were anesthetized using a mixture of ketamine hydrochloride (40 mg/kg) and xylazine hydrochloride (10 mg/kg) via intramuscular administration. A heating pad was used to maintain a constant body temperature of 37 °C. ABR recordings were performed for both ears using a real-time signal processing system (Tucker-Davis Technologies [TDT], System RZ-6, Alachua, Fl, USA, 195,312-Hz sampling rate). The system output was calibrated before the recordings, using a one-quarter inch microphone (Bruël and Kjaer). Three subcutaneous needle electrodes placed at the vertex (reference electrode), the mastoid ipsilateral to the stimulated ear (active electrode), and the mastoid contralateral to the stimulated ear (ground electrode) were used for the recordings. Sound stimuli consisted of a 5 milliseconds (ms) window, with 1 ms pre-stimuli period, and a 0.1 ms alternating polarity click, with a repetition rate of 21 bursts/s, delivered in 10 dB ascending steps from 10 to 90 dB (Sound Pressure Level, SPL). The stimuli were delivered in close field using a magnetic speaker (TDT, MF1 Multi-Field Magnetic Speakers) connected to the external auditory meatus of a single ear through a 10 cm long plastic tube. This approach resulted in a total delay of 1.4 ms in stimulus arrival at the tympanic membrane. An ABR was obtained by averaging 1000 EEG responses to 1000 click stimuli. Evoked potentials were amplified and digitized using a Medusa RA16PA preamplifier and RA4LI headstage. The final signal was filtered with a 500 Hz high-pass filter and a 3000 Hz low-pass filter.

The ABR analysis was done using a custom-made script developed in MATLAB software (version R2014a, The MathWorks, Inc). The quality of each recording was assessed measuring the mean background voltage of the 1 ms period before the stimulus onset. The ABR threshold was defined as the stimulus level that evoked a mean voltage value greater than 2 times the standard deviation above the mean background activity. These auditory thresholds were confirmed by blind visual inspections at the lowest intensity at which waves I and II were detectable above noise within the 5 ms response window immediately before the stimulus onset. The amplitude and latency of click ABR waves were measured at the suprathreshold hearing level of 90 dB SPL, analyzing positive and negative peaks of each wave with the MATLAB program. Wave amplitude was defined as the sum of the positive and negative peak values of each wave. The absolute wave I latency was defined as the time in ms from the stimulus onset to the positive peak of the wave. The inter-peak latencies were defined as the time in ms between the positive peaks of the different ABRs waves. All animals used for ABR measurements were processed for cochlear histology and immunohistochemistry.

2.3. Cochlear histology

After the ABR hearing measurements, animals were perfused through the aorta with aldehydes following the procedures described by Sánchez-Benito et al. (2017). The temporal bones of 2 control and 2 GASH/Sal hamsters were removed from the head. The bulla was opened, and the cochlea was dissected under the microscope and perfused through the round window with a fixative containing 4% paraformaldehyde in 0.1 M phosphate buffered saline (PBS), pH 7.4 solution, and subsequently immersed in the same fixative solution for 1 day. The cochleae were then decalcified in 10% ethylenediaminetetraacetic acid (EDTA) for 1 week, and embedded in paraffin. The paraffin-embedded cochleae were sliced along the mid-modiolar axis into sections of 6 μm thick, mounted on silane-coated slides and stained with cresyl-violet (Nissl stained). The serial sections were studied using a Leitz DMRB (Leica) light microscope equipped with digital camera, and the cochlear turns were divided into three regions: apical, middle and basal for histology image analysis, SGNs quantification and SV thickness measurements.

2.4. Quantification and morphometric analyses of SGNs and SV

Quantification and morphometry of spiral ganglion neurons (SGNs) and stria vascularis (SV) were carried out in light microscope images of 4 cochleae (corresponding to 2 control and 2 GASH/Sal animals), using the open source software ImageJ (v1.51g-v1.51n; Fiji package). Spiral ganglion cells were counted using a 20x objective lens. The corresponding area of the Rosenthal's canal was measured in digital photomicrographs of each canal profile (apical, middle and basal). The perimeter of the canal was traced with a cursor using ImageJ program. The computer then calculated the area within the outline. Density was calculated as the number of SGNs per mm^3 as described elsewhere (Keithley and Feldman, 1979; Nadol, 1988) in every two sections of the entire cochlea. SGNs were included in the counts if their nuclei were visible in the section. Since the heterochromatin visible in the nucleus was sometimes mistaken for the nucleolus, nuclei were counted instead of nucleoli (Berglund and Ryugo, 1991). Type I and type II SGNs were not differentiated and all counts were corrected for split-cell error by the Abercrombie formula, with the assumption that the nuclei were spherical [corrected count = (nuclei counts x section thickness)/(section thickness + nuclear diameter); Abercrombie, 1946]. The nuclear diameter was determined by morphometric analyses of 486 nuclear cross-sections at 40x objective lens. The mean nuclear diameter was 7.1 ± 0.71 μm (n = 255) for controls and 6.9 ± 0.68 μm (n = 231) for GASH/Sal hamsters and these values were the same for all regions of the cochlea. In addition, cross-sectional areas, perimeter and roundness of SGNs somata were measured using the ImageJ software as described by Sánchez-Benito et al. (2017). A total of 834 SGNs (417 in each animal group) corresponding to different region of the cochlea were imaged at 40x objective lens and their somata measured while taking care not to include the satellite glial cells. The number of strial blood vessels and SV thickness were analyzed in digital images of Nissl-stained cochlear tissues acquired with a 20x objective lens. A total of 304 stria vascularis (134 for controls and 170 for GASH/Sal animals) corresponding to the apical, middle, and basal turns of the cochlea were evaluated with the ImageJ software. Capillaries in the SV that included endothelial cells were considered as a count. The measurement of SV thickness was made by using a cursor to draw a line from the margin of the SV to the junction of the basal cells with the spiral ligament half-way between the attachment of Reissner's membrane and the spiral prominence (Keithley et al., 2005). This measured line corresponding to the SV

thickness matched the perpendicular bisector of the reference structures. All quantification analyses were carried out in a single-blind assessment by two different investigators.

2.5. Scanning electron microscopy analyses and stereocilia counts

For the scanning electron microscopy study, the cochleae of 2 control and 2 GASH/Sal hamsters were processed following the procedure described by Sánchez-Benito et al. (2017). The animals were anaesthetized with sodium thiopental (Abbott) (69 mg/kg) and perfused transcardially with 0.1M phosphate buffer solution, followed by 4% paraformaldehyde and 0.1% glutaraldehyde in 0.1 M of phosphate buffer (pH = 7.4), using a speed-controlled pump perfusion Masterflex® (Paste, Parmer). Each temporal bone with its tympanic cavity was removed by exposing the tympanic bulla and then opened for cochlear exposure. The two cochleae of each animal were dissected under the microscope and gently perfused in 4% paraformaldehyde solution and subsequently maintained in the same fixative solution for 4 h. Cochleae were placed in 1% OsO_4, dehydrated with increasing concentrations of ethanol and critical point dried from CO_2. Dried samples were mounted on metal support stubs and then sputter coated with gold. The observation and analysis of the cochlear hair cells were carried out with an Electron Microscope JEOL SCANNING MICROSCOPE — JSM 5200. To map the results of our analysis, we divided the cochlea into several regions, with the base of the cochlea closest to the stapes and the apex or apical region at the tip of the spiral. Digital images of the basal, middle and apical cochlear turns were obtained at a magnification that ranged from 2,000x to 5,000x. The total number of stereocilia per hair cell was obtained by counting the number of stereocilia tips present in the tallest row of a given tuft. Hair cells that lose all or almost their entire stereocilia tuft were not included in the stereocilia analysis. A total of 27 IHCs and 57 OHCs were counted in each group of animals (n = 168). In addition, morphometric data of stereocilia and blebs (length in microns) was obtained from images taken with the same angle to the apical surface of the hair cell at a magnification of 5,000x using the ImageJ program.

2.6. Real-time quantitative PCR (RT-qPCR)

The cochlea of 6 control and 6 GASH/Sal hamsters were collected to study the differential expression of the following cochlear genes: *Prestin*, *Cdh23*, *Pcdh15*, *Vglut1*, and *Vglut2*. Tissue samples containing the entire cochlear nucleus of those animals were also used to perform differential gene expression analysis of *Vglut1* and *Vglut2*. The cochleae and the cochlear nuclei of each animal were obtained following euthanasia by deep anesthetization and rapid decapitation. Each cochlear nucleus was frozen immediately in liquid nitrogen and each cochlea was transferred into the Trizol reagent (Gibco BRL, Gaithersburg, MD, USA). The oval window and the apex of the cochlea were opened immediately to let the Trizol reagent enter the cochlea as soon as possible. The samples were stored at −80 °C until RNA extraction. The RT-qPCR approach was identical to that used previously by our group (e.g. Damasceno et al., 2020). Total cellular RNA from frozen tissue was extracted from the individual tissue samples using the Trizol reagent in accordance with the manufacturer's procedure. The quantity and quality of total RNA were verified by optical density using the NanoPhotometer® spectrophotometer (Implen GmbH), taking into account the absorbances ratios 260/280 and 260/230 nm, and the RNA integrity was checked by electrophoresis in agarose gel (1.5%).

Complementary DNA (cDNA) was synthesized from 800 ng of total RNA using the ImProm-IITM Reverse Transcription System Kit (Promega Corporation, Madison, SWI, USA) according to the manufacturer's instructions. The RT-qPCR analysis was performed using the QuantStudio 7 Flex System (Applied Biosystems by Life Technology, Europe) with the Power SYBR Green PCR Master Mix (Applied Biosystems by Life Technologies, Europe). 20 μl PCR mixture contained 80 ng of cDNA template, 400 nMol of each primer and 10 μl of Power SYBR Green PCR Master Mix. Table 1 shows the specific primers for the genes examined in the present study, which were designed in such a way that RT-qPCR products spanned two identified introns (for more details on the primer design methodology, see Damasceno et al., 2020). PCR amplification was as follows: 10 min at 95 °C before 40 thermal cycles, each consisting of denaturation at 95 °C for 15 s and annealing/extending at 60 °C for 30 s, followed by melting curve. Output data were analyzed with QuantStudio™ Real-Time PCR software (v. 1.3; Applied Biosystems by Thermo Fisher Scientific) and were normalized by beta-actin (β-actin) expression. The relative gene expression value of each transcript was calculated following the comparative $2^{-\Delta\Delta Ct}$ method as used previously (Damasceno et al., 2020). Finally, a negative template-free (water) control reaction was used in all RT-qPCRs and the control group was used as the calibration sample.

2.7. Antibody characterization

In this study, we used immunohistochemistry to determine the distribution of the vesicular glutamate transporter 2 (VGLUT2) in the cochlear nucleus of control and GASH/Sal hamsters. We used polyclonal antibodies generated in rabbits against Strep-Tag fusion protein containing amino acid residues 510−582 of rat VGLUT2 (catalog No. 135 402; Synaptic Systems). This recombinant protein from rat VGLUT2 has been tested in preadsorption experiments that blocked efficiently and specifically the corresponding signals (manufacturer's technical information). In Western blots analysis of cerebellum and cochlear nucleus, the rabbit polyclonal antibodies for VGLUT2 recognize a single band migrating at ~65 kDA, respectively (Zhou et al., 2007). This primary antibody has been successfully used in previous studies to immunolabel VGLUT2 axon terminals in the cochlear nucleus of guinea pig (Zhou et al., 2007), rat (Gómez-Nieto and Rubio, 2009) and monkey (Gómez-Nieto and Rubio, 2011). According to the manufacturer's technical information, the reactivity has not been tested yet in hamster brain tissue. Thus, a multisequence alignment analysis was developed firstly to determine the variability or conservation of epitopes in the hamster. To do this, the VGLUT2 protein sequences corresponding to the Slc17a6 gene were retrieved from the NCBI protein database (http://www.ncbi.nlm.nih.gov/protein/), and then analyzed using the EBI-Clustal Omega program (http://www.ebi.ac.uk/Tools/msa/clustalo/) (Sievers and Higgins, 2018). The multiple sequence alignment showed that the epitope sequence, antigenic region, is highly conserved for all VGLUT2 isoforms in the hamster (Supplemental Material 1).

2.8. Brain tissue processing and immunostaining

Brain tissue used for immunohistochemical analysis was obtained from the animals previously tested for ABR (4 control and 4 GASH/Sal hamsters). After injection of a lethal dose of sodium pentobarbital (60 mg/kg) and the subsequent perfusion through the heart with 4% paraformaldehyde in 0.1 M PBS, brains were removed from the skull, cryoprotected by immersion in 30% sucrose, and coronal sections were cut with a freezing sliding microtome at 40 μm thickness (Sánchez-Benito et al., 2017). Serial sections were collected in PBS and divided into series of 6, 3 of which were for light microscope immunohistochemistry and the

Table 1
List of primers used for RT-qPCRs.

Target gen	Primer Forward	Primer Reverse	Size of products (pb)	Temp (°C)
Vglut1 (*Slc17a7*)	ACCTGTTCTGGTTGCTCGTC	CGTAGACTGGCATGGATGTG	184	60
Vglut2 (*Slc17a6*)	CTTTGGCATGGTCTGGTACA	ACGGGGTCTTGAATTTTTCC	155	60
Prestin (*Slc26a5*)	TCGCCATGTCTGTGACCTTA	CCCACTGTACCGCTTTGTTT	185	60
Cadherin 23 (*Cdh23*)	ATCCAAGTTGGAGATGTGAATGAC	GTTGACGATGAAGATGGGTGTC	108	60
Protocadherin 15 (*Pcdh15*)	AGTTCTGGATAGAGACCCACCA	ATAACTGTGCCCACCTTCTTGT	84	60
β-actin	AGCCATGTACGTAGCCATCC	ACCCTCATAGATGGGCACAG	115	60

other 3 for immunofluorescence. The VGLUT2 was visualized following the indirect method of immunohistochemical staining described by Gómez-Nieto et al. (2008b). All immunostaining steps were performed at room temperature (~22 °C), unless otherwise stated. Washes were made in Tris-buffered saline (TBS), pH 7.4 and dilutions of antisera in TBS containing 0.2% Triton X-100 (catalog No. T9284; Sigma). For light microscopy analysis, free-floating sections were blocked for 1 h with 5% normal goat serum (catalog No. S-1000, Vector Labs.) in TBS-Tx and were incubated with primary antibodies, rabbit anti-VGLUT2, at 1:1000 dilution for 72 h at 4 °C. Sections were then washed and followed an incubation with the biotinylated secondary antibodies, goat anti-rabbit (catalog No. BA-1000, Vector Laboratories), at 1:200 dilution for 2 h. After removal of secondary antisera, the visualization of epitope-antibody interactions was developed with the avidin-biotin-peroxidase complex procedure (catalog No. PK-4000, Vectastain, Vector Labs.), and diaminobenzidine histochemistry for peroxidase without heavy-metal intensification (DAB Kit, catalog No. SK-4100, Vector Labs.). All sections were mounted on slides, dehydrated and coverslipped with Entellan® Neu (catalog No. 107961, Merck). For immunofluorescence analysis, brain sections followed the blocking with 5% fetal calf serum (Sigma) and incubation with primary antibodies as described above. Thereafter, the sections were rinsed extensively and reacted for 2 h with secondary antibody (Cy2 donkey anti-rabbit, catalog No. 711-225-152, Jackson Immunoresearch) at 1:200 dilution for 2 h. Finally, sections were mounted on slides and coverslipped with VECTASHIELD® mounting medium for preserving fluorescence, containing the DAPI counterstain (4′,6-diamidino-2-phenylindole, catalog No. H-1200, Vector Labs.).

An additional control hamster was processed to study the morphology of the hamster cochlear nucleus to distinguish its subdivisions. Brain tissue of this animal was processed as described above to obtain coronal and parasagittal sections of 40 μm thickness. Brain sections containing the cochlear nucleus were collected in PBS and divided into 2 series. The first series was processed following the Nissl-staining method to reveal the cytoarchitecture of different cochlear nucleus regions. The second series was stained with the fluorescent DAPI dye that labels the nuclear DNA of cells to precisely identify cytoarchitectonic borders of the cochlear nucleus subdivisions.

In another set of experiments, we studied the morphometric features of VGLUT2-immunolabeled terminals in the cochlear nucleus. For this purpose, 2 control and 2 GASH/Sal hamsters were used. The brain tissue was obtained as described above and embedded in paraffin wax before being cut into coronal sections of 6 μm thickness. Then, sections were mounted onto slides and followed the immunohistological staining procedure to visualize the VGLUT2 protein using the EnVision FLEX Mini Kit, High pH (catalog No. K8023, Dako). After deparaffinization and rehydration, endogenous peroxidase activity was blocked using EnVision FLEX peroxidase-blocking reagent (catalog No. SM801, Dako) for 6 min. Sections were blocked with 5% normal goat serum in TBS-Tx for 1 h, and incubated with primary antibodies, rabbit anti-VGLUT2, at 1:1000 dilution for 24 h. After washing, sections were then incubated with EnVision Flex linked with horseradish peroxidase (catalog No. SM802, Dako) for 30 min, and the staining was visualized by using the substrate DAB chromogen mix (catalog No. SM803/DM827, Dako). Finally, the sections were counterstained with Carazzi's hematoxylin, dehydrated and cover slipped with DPX Mountant (Sigma). In all immunohistochemical experiments, omission of primary antibody resulted in no positive staining of the preparations. Because VGLUT2-immunoreactivity is well documented in the cerebellar cortex (Hioki et al., 2003; Miyazaki et al., 2003; Zhou et al., 2007), we used the cerebellum as the positive control. The staining patterns for immunohistochemistry and immunofluorescence using VGLUT2 antibody in the cerebellar cortex of the hamster were almost the same as those described in other rodent species (Supplemental Material 2).

2.9. Image acquisition and VGLUT2 analysis

Digital images used for illustration and VGLUT2 analysis were taken from well-defined cytoarchitectonic subdivisions of the cochlear nucleus in control and GASH/Sal animals. All microscope parameters and settings for digitizing the photomicrographs remained constant across both experimental groups and for each animal. The sections processed for light microscopy were studied using a Leitz DMRB (Leica) light microscope coupled with digital camera. Low-magnification images were taken with the 4x or 20x objective lens, and high magnification images were taken with a 40x or 100x objective lens (oil immersion). Images of 6-μm coronal sections at 100x magnification were analyzed through the cochlear nucleus subdivisions to measure the size (area in μm^2) of 482 labeled puncta by tracing their contours using ImageJ software as described elsewhere (Gómez-Nieto et al., 2008a). The sections processed for immunofluorescence were studied on a Zeiss Axio Observer.Z1-Inverted Microscope with ApoTome optical sectioning system (Zeiss) using the appropriate filters for Cy2 and DAPI fluorochromes. Quantification of VGLUT2-immunolabeled puncta was carried out in fluorescence microscopy images that were taken in a single optical plane with a plan-apochromat 63x objective (NA-1.4) using the Multicolor module of AxioVision (Zeiss) with identical image acquisition settings and exposure times. The total number of fluorescence images analyzed was 542, ranging from 16 to 28 in each case (3 control and 3 GASH/Sal hamsters) and each cochlear nucleus subdivision. The analyzed areas had an average of 0.015 mm^2 and included caudal to rostral regions for each of the cochlear nucleus subdivisions. The procedure to count VGLUT2-immunolabeled puncta in fluorescence images using the ImageJ software is shown in the supplemental material 3. To ensure reliable counting, visual inspections were conducted after each automated count (Supplemental Material 3). This procedure was performed by two independent investigators in a single-blind assessment of the samples. The number of puncta was divided by the chosen area to yield the density of puncta per unit area (in mm^2) and corrected for double-counting errors with the Abercrombie formula. Representative images for illustration were collected as stacks with a z-step of 0.25 μm slices with 5x and 63x

objective lenses, and were showed as the maximum intensity projection images of 5 μm thick.

2.10. Image editing and statistical analysis

Representative images shown in the figures were processed by minor modifications with regard to brightness and contrast using ImageJ software and the final figures were composed with Canvas 14. Statistical analyses of ABR amplitudes and latencies, relative gene expression values, morphometric features such as area, perimeter, length and roundness as well as quantification of hair cell stereocilia, SGNs and VGLUT2-puncta were performed using the SPSS-IBM software, version 20 (SPSS Inc., Chicago, IL, USA). All quantitative data were expressed as mean value ± standard error of the mean (SEM). For each statistical analysis, comparisons between control and GASH/Sal animals were performed with analysis of variance (post-hoc analysis with Fisher's test) and Student's *t*-test. The differences were considered statistically significant with a p value < 0.05 (*), p value < 0.01 (**) and p value < 0.001 (***).

3. Results

3.1. Evaluation of hearing function

To estimate hearing sensitivity and to identify neurological abnormalities of the auditory nerve and the auditory pathway up through the brainstem of the GASH/Sal, we compared ABR differences between control and GASH/Sal hamsters with respect to ABR thresholds as well as waves amplitudes and latencies. The two animal groups showed five clear peaks of ABR (waves I to V) in response to clicks of the maximum testing intensity (90 dB SPL) after stimulation of the left and right ears. Examples of ABRs are shown in Fig. 1A. The means ± SEM of the ABR threshold in control and GASH/Sal hamsters were 28.7 ± 3.5 dB SPL and 75 ± 9.3 dB SPL, respectively. Statistical comparisons showed that the average ABR thresholds of GASH/Sal hamsters were significantly higher than ABR thresholds of age-matched control animals for left and right ears ($p < 0.001$; Fig. 1B). Differences in amplitudes of the ABR waves were also found between the control and GASH/Sal hamsters (Fig. 1A, C and 2A). The statistical analysis of ABR amplitudes (peak to peak) at 90 dB SPL showed that wave I and IV were significantly lower in the GASH/Sal than in the control hamster ($p < 0.01$; Fig. 1C). However, there were no significant differences in ABR amplitudes for waves II, III and V between the two animal groups (Fig. 1C). The GASH/Sal showed absolute latencies of all waveform components, waves I through V, very similar to those in control animals, and no statistically significant differences were found (Fig. 1D). The inter-peak latency of ABR waves did not show any statistically significant differences between the two animal groups (Fig. 1E). The ABR analysis showed that the auditory function of GASH/Sal animals is impaired at 4 months old, exhibiting very high auditory thresholds with a pronounced decrease in the amplitude of wave I, which was accompanied by an equivalent significant decline of wave IV.

3.2. Cochlear histopathology

The elevated ABR threshold and reduced wave I amplitude in the GASH/Sal might be associated with auditory nerve fibers reductions, reflecting possible pathological alterations in the cochlea. In order to investigate whether these ABR abnormalities in the GASH/Sal correlated with morphological defects in the cochlea, a histological study was performed after ABR testing (Fig. 2A). Same as in the control group, the cochlear microscopic structure of the GASH/Sal animals in a cross section from the base to the apex showed preservation of the Reissner's, basilar and tectorial membranes as well as normal appearance of cochlear turns without apparent loss of sensory hair cells (Fig. 2B–G). However, alterations in the organ of Corti, the spiral ganglion cells and stria vascularis were found in all GASH/Sal animals that exhibited a decline of ABR wave I amplitude (Figs. 2–4). In the organ of Corti of control animals, the supporting cells and hair cells with stereocilia bundles were identified with clear cell definition (Fig. 2D and F). In contrast, GASH/Sal animals showed complete absence of stereocilia bundles in the IHCs and OHCs as well as morphological alterations in supporting cells (see Fig. 2F and G for comparison). Since the major site of cochlear pathology frequently includes auditory neurons in the the spiral ganglion, we also assessed the number of SGNs in the basal, middle and apical regions of the cochlea from the same animal groups (Fig. 3). A generalized reduction of SGNs was observed in Nissl-stained sections of the GASH/Sal cochlea. In contrast to the control spiral ganglion (in which SGNs were tightly packed), the SGNs in the GASH/Sal were scattered in the entire cochlear modiolus (Fig. 3A). These qualitative differences of neuronal loss in the GASH/Sal animals were confirmed by counting the SGNs in each profile of the Rosenthal's canal. The mean SGN density of GASH/Sal animals was significantly lower than that of control animals for each cochlear region of the spiral ganglion ($p < 0.001$; Fig. 3B). Compared to controls, the following regional percent decreases were obtained in the GASH/Sal: apex (37.8%), middle (43.3%), and base (41.4%), indicating that these losses are occurring uniformly along the length of the spiral ganglion. The mean total density of SGNs per mm^3 was 189.4×10^3 (SEM = ± 33.9) for control animals and 112.1×10^3 (SEM = ± 24.9) for GASH/Sal animals. These decreases in density might be caused by either a decrease in the number of SGNs or by an increase in the volume of the canal, thus we analyzed the canal volume measurements in both animal groups. The mean total volume of the canal measured in controls and GASH/Sal animals was 0.0083 mm^3 (SEM = ± 0.0015) and 0.0084 mm^3 (SEM = ± 0.0011), respectively, and the mean volume of the canal in each cochlear region was not significantly different in the two groups of animals (Supplemental Material 4). This indicates that the density differences between controls and GASH/Sal animals were due to changes in number of SGNs, rather than in the volume of the Rosenthal's canal. Another feature that might contribute to the differences observed in the ABR waveforms is the cell size and shape of SGNs. In controls animals, Nissl-stained sections of the spiral ganglion allowed to distinguish between the both types of SGNs (Supplemental Material 5). Type I neurons had a larger cell body with prominent Nissl bodies in their cytoplasm, and a pale staining nucleus. Type II neurons were distinguished by their small somatic size and pale cytoplasm. In the GASH/Sal, SGNs occasionally exhibited pyknotic nuclei and shrunken cell somata, and hence, distinguishing between the two types of SGNs was not possible (Supplemental Material 5). In both animal groups, a satellite glial cell was frequently observed in the side of the cell bodies of SGNs (Fig. 3A and Supplemental Material 5). Thus, in order to quantify changes in neuronal size, the cross-sectional areas of SGNs were measured along the length of the spiral ganglion, regardless of the cell type and without including the satellite glial cell. The differences in the area and perimeter of spiral ganglion cell bodies were statistically significant when compared control and GASH/Sal hamsters ($p < 0.001$; Fig. 3C). Relative to controls (mean area of 91.9 ± 16.3 μm^2 and perimeter of 34.8 ± 3.1 μm), the cross-sectional area and perimeter of SGNs in the GASH/Sal exhibited a percentage reduction of 20.4% and 10.6%, respectively. Furthermore, we measured the roundness of SGNs in the control and GASH/Sal hamsters. Although the mean values of soma roundness were slightly reduced in the GASH/Sal, we found no statistically significant difference (Fig. 3D). Since atrophy of the SV is a common cause

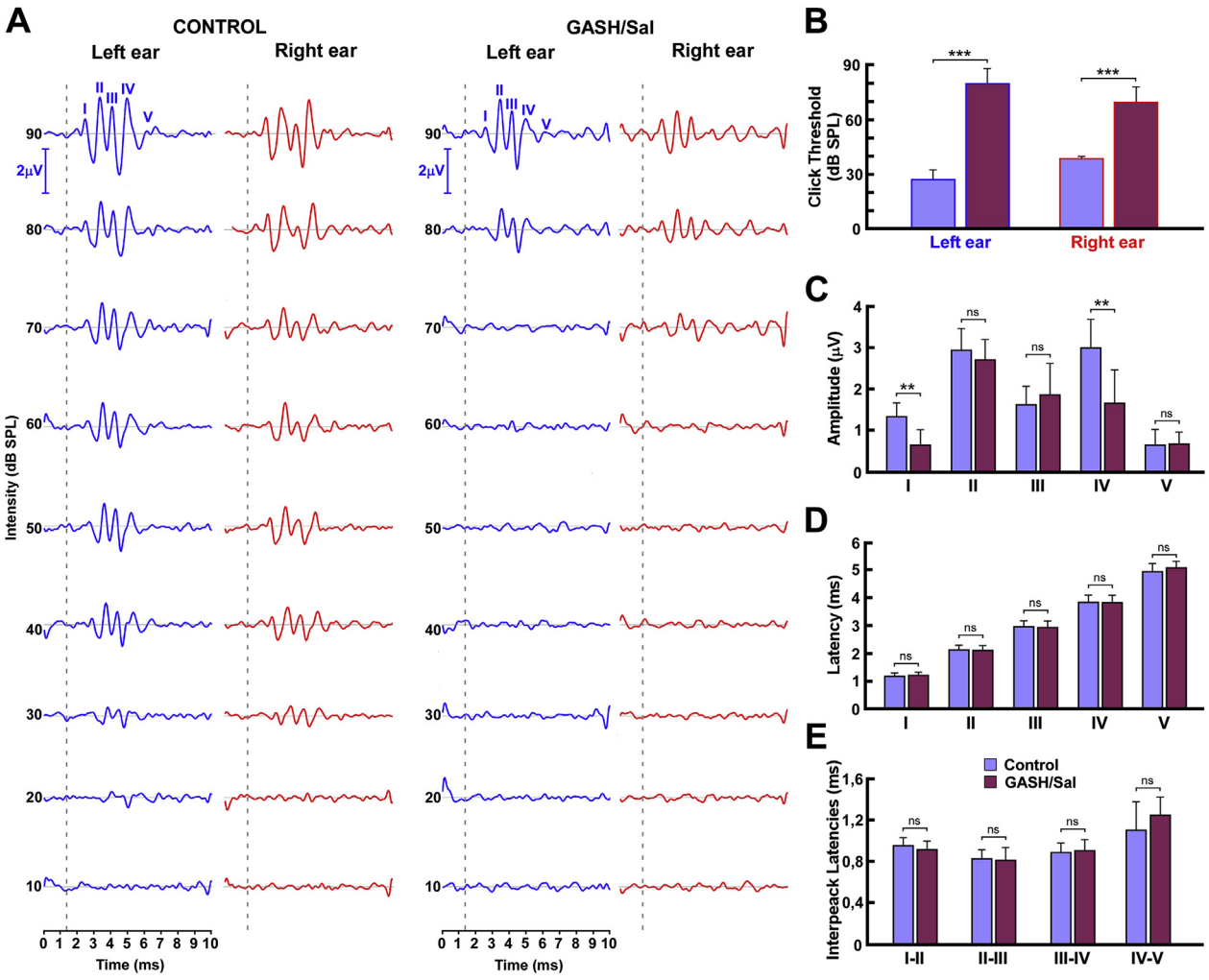

Fig. 1. ABRs differences between the control and GASH/Sal hamsters. **A**. Plots show a representative example of the ABR waveforms obtained from control and GASH/Sal hamsters after click stimulation on the left (in blue) and right (in red) ears. ABR waveforms (amplitude in μV) were recorded from 10 to 90 dB SPL along the first 10 ms. The stimulus onset starts at 1.4 ms. Notice that waves were visible at 30 dB SPL for the control animal, whereas the GASH/Sal's waveforms were visible at 70 and 80 dB SPL for the right and left ears, respectively. Note that waves amplitudes in the GASH/Sal animal were smaller than in the control hamster at suprathreshold levels. **B**. Plot shows ABR thresholds to clicks for the two animal groups (control and GASH/Sal) after stimulation on the left and right ears. Note that ABR thresholds were significantly lower in GASH/Sal hamsters. **C**. Plot shows ABR amplitudes in microvolts (μV) for each waveform responses (I, II, III, IV and V) measured at 90 dB SPL in the two animal groups. Notice that mean values of waves I and IV were significantly lower in the GASH/Sal. **D**. Plot displays latencies for each waveform responses in the two animal groups. Notice that there were no significant differences between the control and GASH/Sal hamsters. **E**. ABR mean inter-peak latencies in ms for the control group compared to GASH/Sal. There were no significant differences between the two animal groups. For histograms B-C-D-E, controls are displayed in blue and GASH/Sal in purple. Graphs display the mean with SEM error bars. "**" = p value ≤ 0.01; "***" = p value ≤ 0.001; ns = non-significant. (For interpretation of the references to color in this figure legend, the reader is referred to the Web version of this article).

for alterations in hearing sensitivity (Schuknecht et al., 1974), we analyzed the cytoarchitecture, the number of blood vessels and the thickness of SV in the apical, middle, and basal regions of the cochlea (Fig. 4). In the control hamster, the SV showed a normal histological organization consisting of three layers of distinct cell types (marginal, intermediate and basal cells) that were highly vascularized by intraepithelial capillaries (Fig. 4A). Although the gross morphology of the SV was apparently conserved in the GASH/Sal, we found traits of mild strial atrophy that included changes in the capillary network and SV thickness as well as absence of strial cells, particularly in the basal and middle cochlear turns (Fig. 4A). Accordingly, the quantitative analyses showed significantly fewer capillaries in all regions of the GASH/Sal cochlea compared with controls (Fig. 4B). In addition, the morphometric measurements indicated a significant reduction in SV thickness in the basal and middle regions of the GASH/Sal cochlea, whereas no significant differences were found in the apical regions (Fig. 4C). Together, these results indicated a reduction of the microvasculature and thickness of the SV in the GASH/Sal cochlea that correlated with abnormalities in the spiral ganglion and cochlear function.

3.3. Scanning microscope study of the reticular lamina

Our histological results suggested defects in the cytoarchitecture of the organ of Corti of the GASH/Sal, including loss of stereocilia in the hair cells and changes in the morphology of cochlear supporting cells. This led us to investigate further the surface of the organ of Corti (the so-called "reticular lamina") along the longitudinal direction of the cochlea using scanning electron microscopy. Control hamsters exhibited the typical ordered cellular pattern of hair cells and supporting cells (Fig. 5 and Supplemental Material 6). The three rows of OHCs were separated from the single row of IHCs by the inner pillar cells (Fig. 5A and Supplemental Material 6A). Both IHC and OHC stereocilia had normal morphology and were observed as

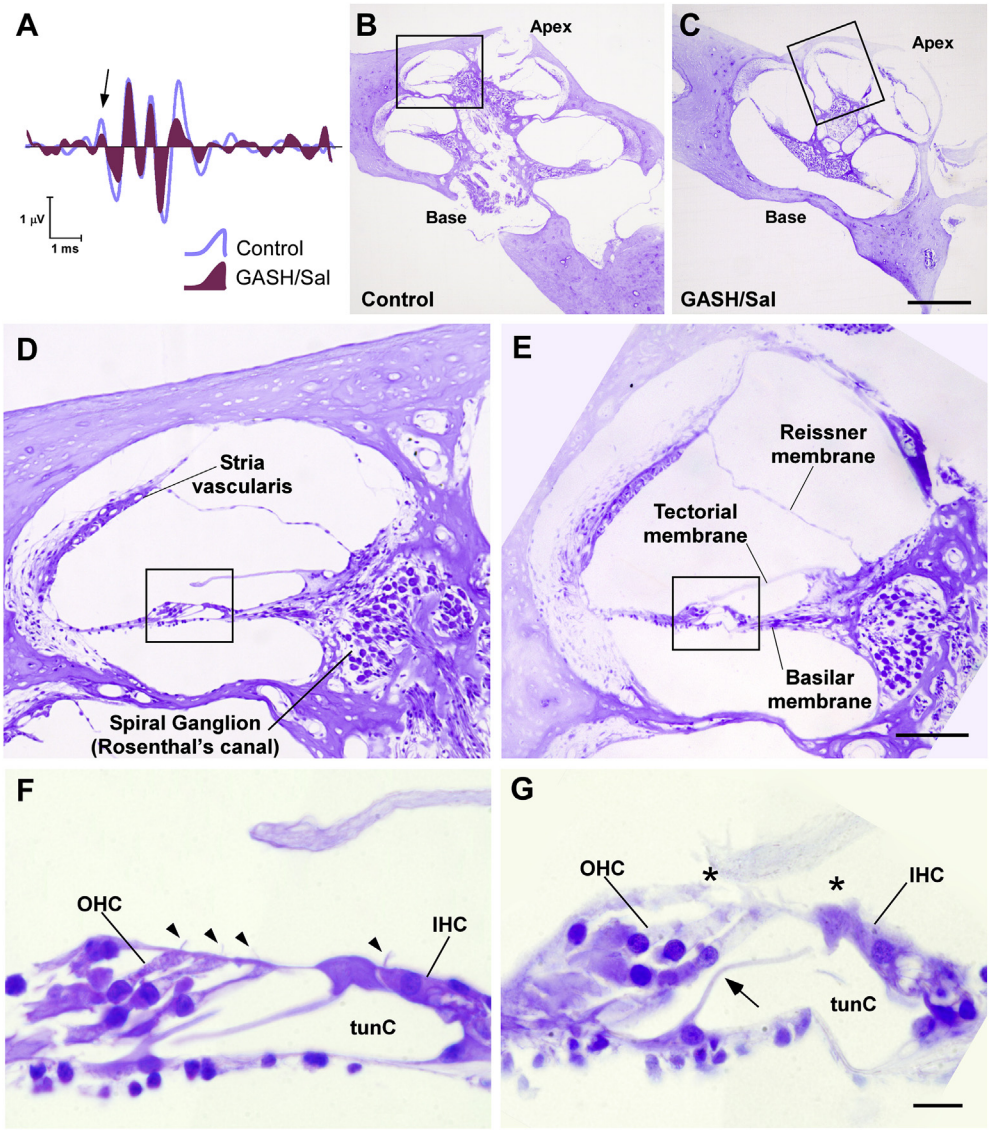

Fig. 2. Cochlea overview of the control and GASH/Sal hamsters. **A**. Representative ABRs in response of click stimulation at 90 dB SPL, corresponding to the cochleae showed in Fig. 2B and C. Notice the reduction in the amplitude of the ABR waveform I (arrow) in the GASH/Sal compared to the control. **B**–**C**. Light micrographs of mid-modiolar Nissl-stained cochlear sections in the control (B) and GASH/Sal (C) hamsters. **D-E**. Higher magnifications corresponding to the frame in B and C show the organ of Corti. Note the Reissner's, basilar and tectorial membranes are preserved in the GASH/Sal. **F-G**. Higher magnifications corresponding to the frame in D and E show inner and outer hair cells (IHC and OHC) in the control and GASH/Sal hamsters. Note that the control animal shows stereocilia (arrowheads) in both IHC and OHC, whereas the GASH/Sal shows missing stereocilia (asterisks). Also, notice the different appearance of the tonofilaments in pillar cells (arrow) enclosing the tunnel of Corti (tunC) in the GASH/Sal. Scale bars = 500 μm in B, C; 100 μm in D, E; 10 μm in F, G.

cylindrical protrusions characterized by highly-organized rows of stereocilia with precise height and width. The stereocilia of IHCs formed a straight or slightly curved bundles (Fig. 5E and Supplemental Material 6A) and the OHC stereocilia formed a V-shaped pattern with a well-defined gradient in height across the stereocilia rows (Fig. 5C and E and Supplemental Material 6B). The reticular lamina of GASH/Sal animals also consisted of a single row of IHCs and three rows of OHCs, however in contrast to controls, a disarray of regular arrangement in three rows of the OHCs were frequently found (Fig. 5B and Supplemental Material 6C). The most noticeable difference compared to control hamsters was the disorganization of stereociliary tufts (Figs. 5 and 6). Such a severe disruption in the regular arrangement of stereocilia was found in both types of hair cells along the entire length of the cochlea (Fig. 6). This stereocilia distortion was frequent in all three rows of the OHCs, and included bents and separations from each other with loss of stereocilia links (Fig. 5D, E and 6). The typical V-shaped pattern of stereociliary tufts was absent in the OHCs of the GASH/Sal (Figs. 5D and 6 and Supplemental Material 6C), and occasionally, their stereocilia appeared to be collapsed (Fig. 6A2-B2-C2). In addition, we frequently found blebs of various size (diameter 0.6–2.1 μm) arising from the cuticular plates of IHCs in all regions of the reticular lamina (Fig. 6A1-B1-C1). Shortening and complete loss of stereociliary tufts were more prevalent in the OHCs than the IHCs, and was particularly more pronounced in the basal turn of the cochlea (Figs. 5D and 6C). To assess changes in stereociliary height and number of stereocilia in the preserved bundles, we measured the length of the tallest stereocilia row and counted their number for each IHC and OHC. Morphometric measurements showed elongated stereocilia in both hair cell types of the GASH/Sal, especially in OHCs with distorted bundle configuration (Fig. 5E and F). Thus, the stereocilia length of IHCs and OHCs in the GASH/Sal were significant greater than in

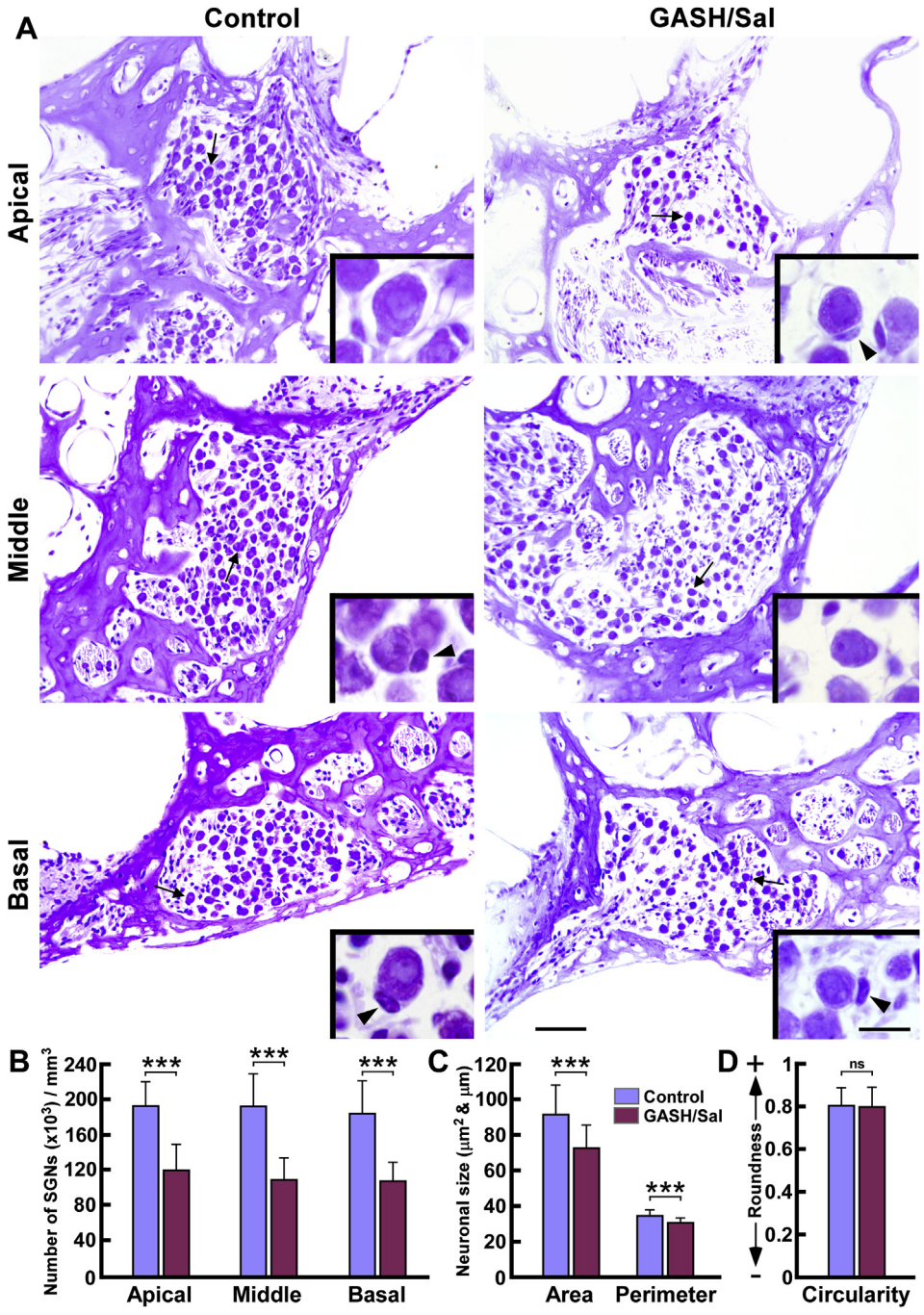

Fig. 3. Quantification and morphometric analyses of spiral ganglion neurons (SGNs) in the control and GASH/Sal hamsters. **A**. Photomicrographs of Nissl-stained sections corresponding to the basal, middle, and apical turns of the cochlea in the control and GASH/Sal hamsters. Insets show details of SGNs somata (corresponding to the arrows in each panel) and the neighboring satellite glial cells (arrowheads). Notice qualitative differences of neuronal loss and somata size in each different region of the GASH/Sal cochlea compared to control hamsters. Scale bars = 50 μm for all panels and 10 μm for insets. **B**. Plot shows the number of SGNs in each different region (apical, middle, and basal) of cochlea tissue. Notice significant loss of SGNs in the GASH/Sal compared to controls. **C**. Histogram shows the area (μm^2) and perimeter (μm) of the cross-sectional areas of SGNs in the control and GASH/Sal hamsters. Notice significant differences in somata size between the control and GASH/Sal hamsters. **D**. Histogram shows the cell roundness of SGNs, where 0 is an infinitely elongated polygon and 1 is a perfect sphere. There was no statistically significant difference in cell roundness between the control and GASH/Sal hamsters. For histograms B-C-D, controls are displayed in blue and GASH/Sal in purple. "***" = p value $\leq$ 0.001; ns = non-significant. (For interpretation of the references to color in this figure legend, the reader is referred to the Web version of this article).

controls, with average increase of a quarter for IHCs and twice the length for OHCs ($p < 0.001$; Fig. 5F). We also found that the stereocilia number for both cell types was significantly lower in the GASH/Sal than in control animals ($p < 0.001$; Fig. 5G). Compared to control animals, the IHCs and OHCs in the GASH/Sal showed a percentage decrease of 24% and 38.3%, respectively. Therefore, changes in morphology and number of stereocilia were more pronounced in OHCs than in IHCs. As a result of such abnormalities in the stereociliary bundles, and because supporting cochlear cells have an important role in degenerative and regenerative events of the hair cells, we also examined the Deiters' cells. In control animals, the cell apex of Deiters' cells extended upward to the reticular lamina in an

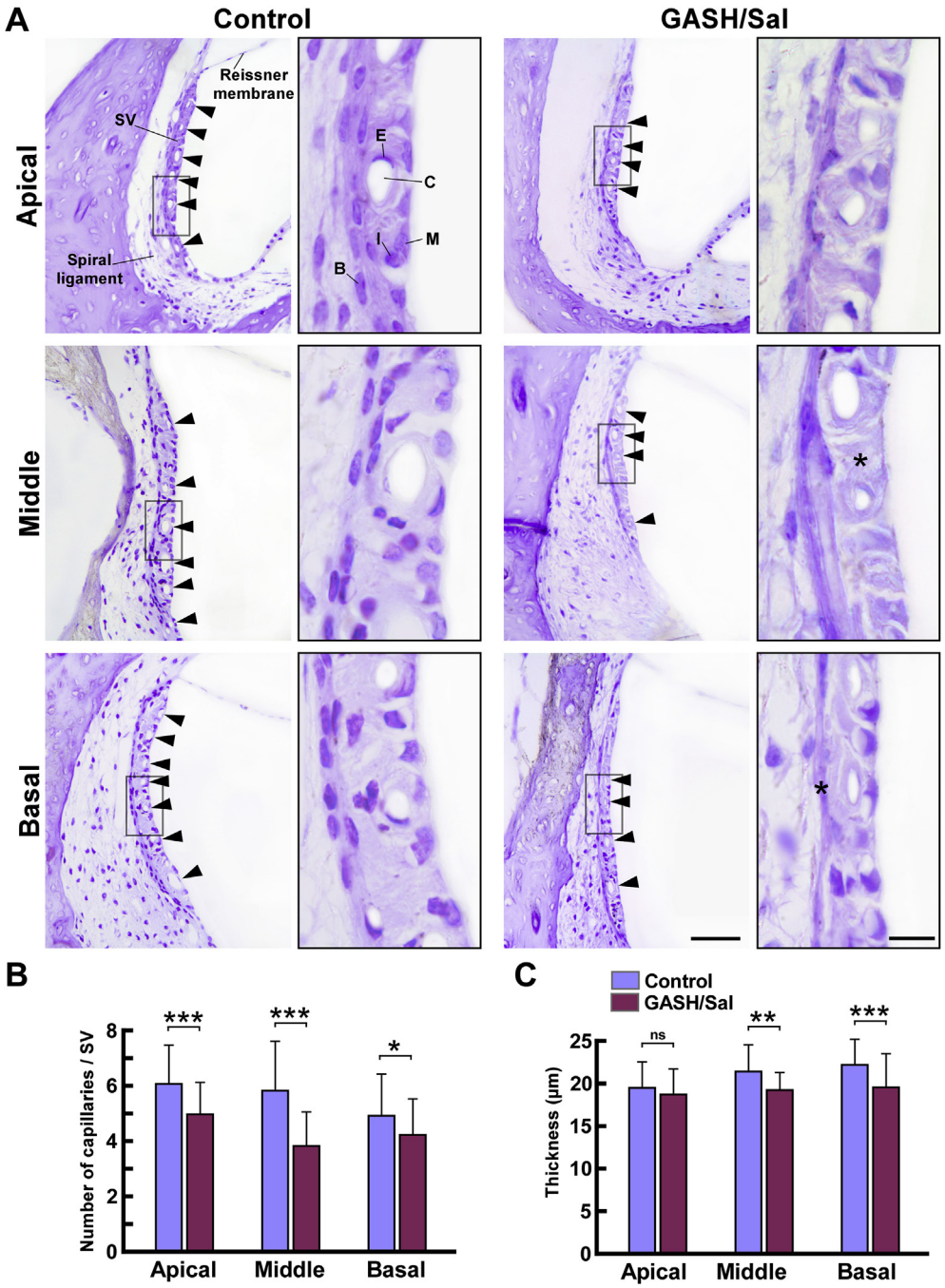

Fig. 4. Comparison of the stria vascularis (SV) in the control and GASH/Sal hamsters. **A.** Photomicrographs of Nissl-stained sections, corresponding to the scala media of basal, middle, and apical turns of the cochlea show representative examples of the SV in control and GASH/Sal hamsters. The area marked by a black square is presented in an adjacent panel with higher magnification to show details of the three layers of cells and capillaries in the SV. Notice lower number of strial capillaries (arrowheads) and lesser SV thickness as well as absence of strial cells (asterisks) in the GASH/Sal when compared to control hamsters. **B**. Plot shows the number of capillaries per SV in each cochlear region (apical, middle, and basal). Note there is a significant loss of vessels in the GASH/Sal compared to controls. **C.** Histogram shows the thickness (in µm) of the SV in each cochlear turn. Notice significant differences in the SV thickness of middle and basal turns between the control and GASH/Sal hamsters. For histograms B and C, controls are displayed in blue and GASH/Sal in purple. "*" = p value ≤ 0.05; "**" = p value ≤ 0.01; "***" = p value ≤ 0.001; ns = non-significant. B, basal cell; C, capillary; E, endothelial cell; I, intermediate cell; M, marginal cell; SV, stria vascularis. Scale bars = 50 µm in low-magnification panels and 10 µm in high-magnification panels. (For interpretation of the references to color in this figure legend, the reader is referred to the Web version of this article).

orderly pattern that distributed in between neighboring OHCs (Fig. 5C and Supplemental Material 6A-B). In contrast to this, Deiters' cells in the GASH/Sal were observed extruding from the apical surface and encroaching into the space of neighboring cells (Fig. 6A and Supplemental Material 6C). These expansions of Deiters' cells were found with increased surface granularity that, at high magnification, appeared as short microvilli (Fig. 6A-A2-B2 and Supplemental Material 6C). Also, the heads of Deiters' cells ended up merging areas of the reticular lamina that showed disarray in three rows of OHCs as well as areas with complete loss of OHC stereocilia (Fig. 6A-B-C and Supplemental Material 6C). Cell bodies of Deiters' cells were preserved in the GASH/Sal as in controls and their phalangeal processes

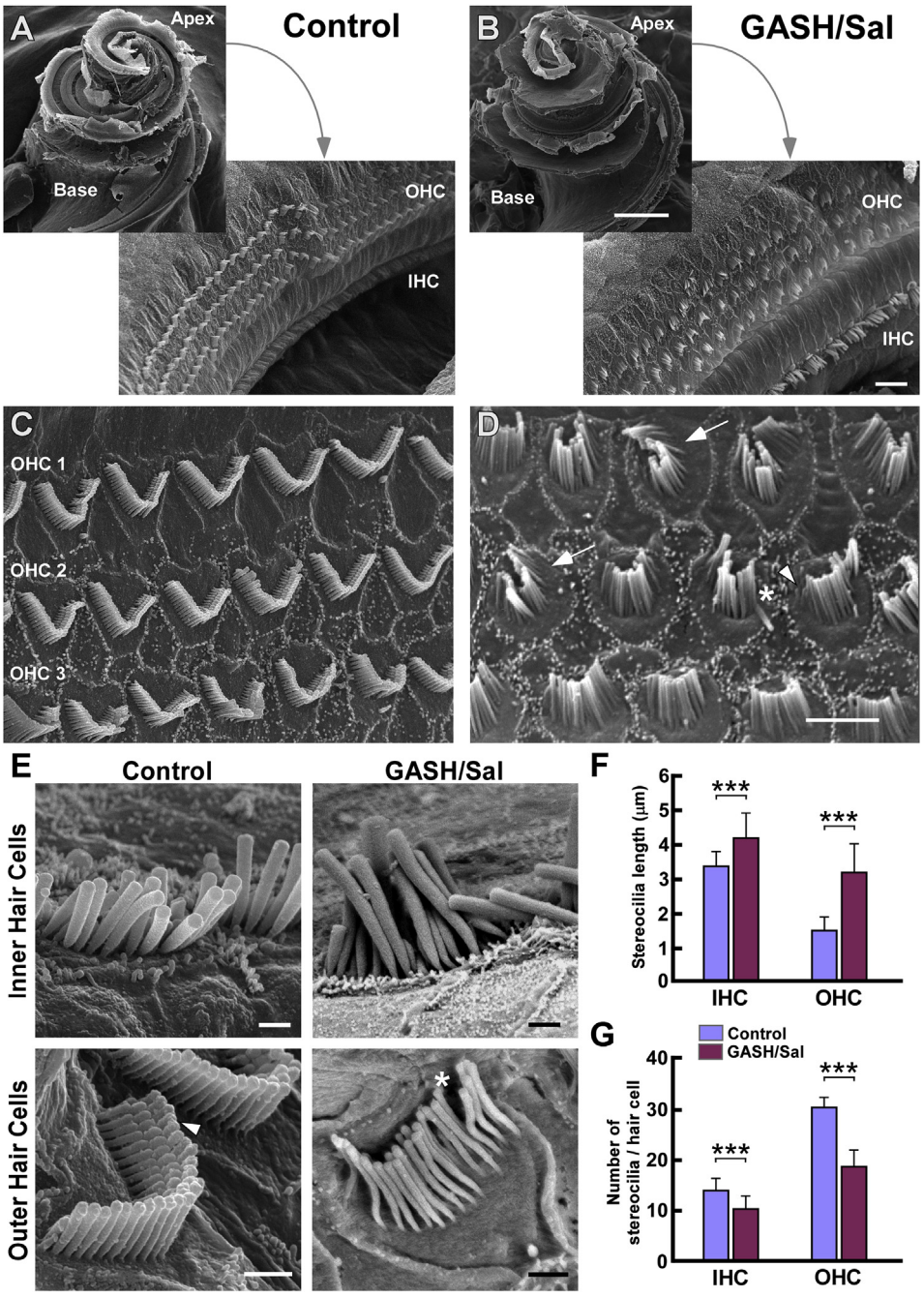

Fig. 5. Scanning electron microscopy (SEM) of the surface of the organ of Corti (reticular lamina) in the control and GASH/Sal hamsters. **A-B**. Low magnification SEM images show the 3 turns of the spiralling basilar membrane supporting the organ of Corti of the control (A) and GASH/Sal (B) hamsters. Higher magnifications of part of the mid-turn of the cochlea showing the orderly rows of inner (IHC) and outer hair cells (OHC). Compare the arrangement of stereocilia in the IHCs and OHCs of the control hamster with that observed in the GASH/Sal. **C-D.** SEM images of the reticular lamina show the three rows of outer hair cells (OHC 1–3) in the control (C) and GASH/Sal (D) hamsters. Compare the V-shape regular pattern of stereociliary tufts in the control cochlea with the disarray of the stereociliary bundles (arrows) in the GASH/Sal. Also, note collapse of stereocilia (asterisk) and shortened stereocilia (arrowhead) in the GASH/Sal. **E.** Higher magnification SEM images show details of stereocilia protruding from the apices of IHC and OHC in the control and GASH/Sal cochleae. Compare the straight or slightly curved bundles of stereocilia in the control IHC with the altered distribution in the GASH/Sal. The control OHC shows linear stereociliary bundles arranged in three rows of graded heights and the links between the stereocilia (arrowhead), whereas the stereocilia of the GASH/Sal OHC are thinner, bent and separated from each other with loss of their links (asterisk). **F.** Histogram shows the mean lengths of stereocilia from the tallest row of the bundle. Notice significant differences in stereocilia length of IHC and OHC between control and GASH/Sal hamsters. Each bar is an average ± S.E.M. of stereocilia from 44 IHC and 62 OHC per animal group. **G.** Histogram shows the number of the tallest stereocilia row per hair cell. Notice significant differences in the number of IHC and OHC stereocilia between the control and GASH/Sal hamsters. Each bar is an average ± S.E.M. of 27 IHCs and 57 OHCs per animal group. For histograms F and G, controls are displayed in blue and GASH/Sal in purple. "***" = *p value* ≤ 0.001. Scale bars = 500 μm in A and B (10 μm for higher magnifications); 5 μm in C and D; 1 μm in E. (For interpretation of the references to color in this figure legend, the reader is referred to the Web version of this article).

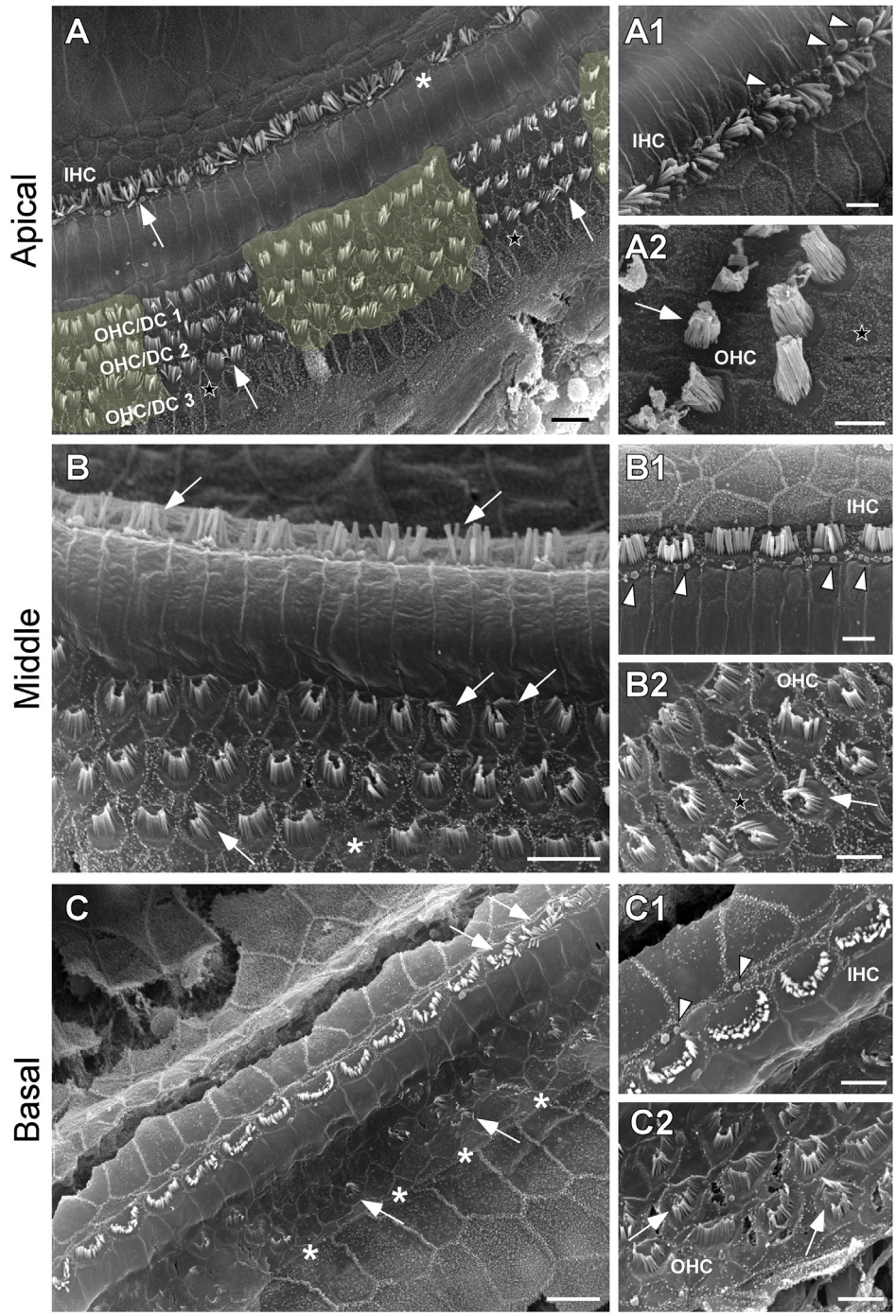

Fig. 6. Scanning electron microscopy of the apical (A), middle (B), and basal (C) turns of the reticular lamina in the GASH/Sal. Notice disarray of regular arrangement in three rows of outer hair cells and Deiters' cells (OHC/DC 1–3, depicted in yellow). Stereocilia distortion (arrows), including bents and separations from each other with loss of stereocilia links are frequent in the three rows of the OHC and in the inner hair cells (IHC). Also, notice the loss of stereociliary tufts and bundles (asterisks), particularly in the basal turn of the cochlea. Higher magnification SEM images show details of the OHC and IHC at the apical (A1-2), middle (B1-2), and basal (C1-2) turns of the GASH/Sal cochlea. Notice frequent blebs (arrowheads) arising from the cuticular plates of IHC. Also, note the increased surface granularity in form of short microvilli (black stars) in the cell apex of supporting cochlear cells. The "V" and "staircase"-like pattern of OHC stereocilia was absent, showing instead shortening, distortion and collapse of the stereociliary tufts (arrows). Scale bars = 10 μm in A, B and C; 5 μm in A1-2, B1-2 and C1-2. (For interpretation of the references to color in this figure legend, the reader is referred to the Web version of this article).

extended obliquely to the reticular lamina (Supplemental Material 6D). Together, these analyses showed an abnormal reticular lamina with peculiar stereociliary defects in the hair cells, thereby confirming our light microscopy observations and suggesting a clear correlation with the loss of functional hearing in the GASH/Sal.

3.4. Disruption in the expression of cochlear genes

To gain further knowledge of the gene expression patterns that underlie the alterations in the cochlear morphology and function of the GASH/Sal, we analyzed mRNA expression levels of the following cochlear genes: *Prestin*, *Cdh23*, *Pcdh15*, *Vglut1*, *and Vglut2*. We

selected these genes, as the proteins they encoded, are essential for the mechanoelectrical transduction and stereocilia integrity in hair cells as well as for the synaptic connection with the cochlear nuclei in the brainstem (Fig. 7A). Whole cochlear tissue containing the sensory epithelium and spiral ganglia were freshly dissected from control and GASH/Sal animals, and a total RNA was extracted immediately. Quantitative gene expression data were normalized using β-actin as internal reference gene. There were no significant differences in the number of cycles to reach the amplification threshold for β-actin with any of the animal groups, indicating that our sample preparation was consistent. Comparison of gene expression/β-actin ratios showed that expression of the all five genes in the GASH/Sal cochleae was significantly lower than in the control cochleae (Fig. 7B). *Prestin* that is responsible of the OHC electromotility showed a marked reduction of mRNA levels in the GASH/Sal compared to controls ($p < 0.001$), a result that correlates to the increased ABR thresholds and the abnormal or absent OHC stereocilia bundles in the GASH/Sal. Expression levels of *Cdh23 and Pcdh15* genes, the tip link constituents that connect stereocilia of a hair cell into a bundle, were also found significantly decreased in GASH/Sal animals versus control hamsters ($p < 0.05$; Fig. 7B). These results were associated with the stereocilia disorganization and loss of tip links observed in the electron microscopy analysis of the reticular lamina. Compared to controls, mRNA levels of *Vglut1* and *Vglut2* genes were severely underexpressed in the GASH/Sal ($p < 0.001$, Fig. 7B). Such a disruption in the expression of genes encoding vesicular glutamate transporters, which are essential for the auditory nerve fibers synaptic connections with the cochlear nuclei, were positively correlated with reductions of ABR wave I amplitudes and the neuronal loss in the spiral ganglion of the GASH/Sal.

3.5. Altered VGLUT2 puncta distribution and Vglut1-2 mRNA expression in the cochlear nucleus

The reduced number of SGNs within the Rosenthal's canal of the GASH/Sal together with the expression imbalance of VGLUTs genes in the cochlea of the GASH/Sal, led us to analyze the distribution VGLUT2-immunolabeling in the cochlear nucleus of the GASH/Sal and compare with that of control animals. As shown in sagittal and coronal sections, the DAPI and Nissl staining allowed us to visualize the morphology of the hamster cochlear nucleus and identify its subdivisions based on cellular characteristics (Fig. 8). The DCN capped the ventral cochlear nucleus, which in turn was divided into two subnuclei, the PVCN and AVCN, at the level of the cochlear nerve root. The granule cell domain (GCD) contained small ovoid cells that formed a continuous layer that covered most of the cochlear nucleus complex along the rostrocaudal axe. Thus, the GCD included granular regions of the DCN layers, PVCN, and AVCN that were clearly differentiated from magnocellular cell areas in each of those subdivisions (Fig. 8). Based on this cytoarchitectural features, we conducted the immunohistochemistry analysis in the following subdivisions of the cochlear nucleus: the DCN (deep and fusiform cell layer), the magnocellular cell areas of the PVCN and AVCN as well as the GCD (Fig. 8C–G). In control animals, VGLUT2-immunolabeling was found differentially distributed throughout the subdivisions of the cochlear nucleus complex. Thus, qualitative light microscope observations of 6-μm coronal sections showed moderate immunolabeling in the DCN, weak immunolabeling in the magnocellular cell areas of PVCN and AVCN, and intense immunolabeling in the GCD (Fig. 9A). In contrast, the GASH/Sal hamsters exhibited strong and intense VGLUT2-immunolabeling in the magnocellular cell areas of PVCN and AVCN, whereas the GCD was weakly immunolabeled (Fig. 9B). VGLUT2-immunolableling was observed as puncta around neuronal cell bodies counterstained with Carazzi's hematoxylin (Fig. 9). At higher magnification, VGLUT2-immunolabeled puncta was found to vary in shape and size throughout the cochlear nucleus subdivisions (Fig. 9). Small-to medium-size *en-passant* endings and large mossy-like endings were found in all subdivisions of the cochlear nucleus complex, with predominance of mossy-like puncta in the GCD (Fig. 9). There were slight differences in the size of VGLUT2-immunopositive puncta between both animal groups. Morphometric measurements revealed that the size (mean area ±SEM) of VGLUT2 *en-passant* endings were 2 ± 0.9 μm^2 (ranging from 0.4 to 4 μm^2) for control hamsters, and 2.2 ± 1 μm^2 (ranging from 0.4 to 4.4 μm^2) for GASH/Sal animals. On the other hand, the size of VGLUT2 mossy-like endings were 8.4 ± 3.6 μm^2 (ranging from 4 to 21.8 μm^2) for controls and 7.1 ± 3.1 μm^2 (ranging from 4.2 to 17.1 μm^2) for GASH/Sal animals. Changes in the distribution of VGLUT2-immunolabeling were also evident in sections of 40-μm thick (Fig. 10). When compared to controls, GASH/Sal animals exhibited a very dense, patchy and disorganized VGLUT2-immunolabeling composed of numerous varicosities, particularly noticeable in the

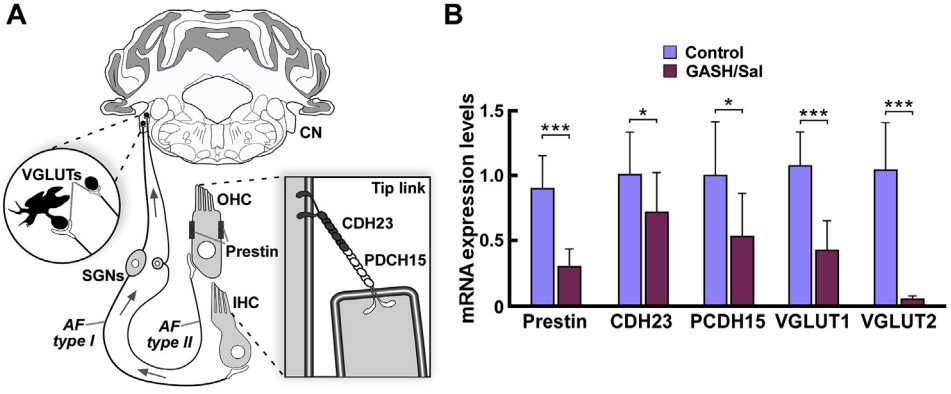

Fig. 7. mRNA expression levels of cochlear genes in the GASH/Sal. **A**. Sketch shows the molecular components of the mechanotransduction machinery that were subjected to gene expression analysis. Notice the location of the corresponding proteins: Prestin, cadherin 23 (CDH23), protocadherin 15 (PCDH15), and vesicular glutamate transporters (VGLUTs: VGLUT1 and 2). Arrows indicate direction of the signal transmission from the inner and outer hair cell (IHC and OHC, respectively) to the cochlear nuclei (CN), via afferent fibers of spiral ganglion neurons (AF type I and type II). **B**. Histogram shows relative quantities of transcripts of the cochlear genes in the control and GASH/Sal animals. The relative mRNA expression of each gene of interest was normalized to β-actin. ΔCt values were normalized to the average ΔCt of the control cochlear tissue. Asterisks indicate significance of the difference in expression of each gene in the GASH/Sal cochleae as compared to the control cochleae. "*" = p value ≤ 0.05; "**" = p value ≤ 0.01; "***" = p value ≤ 0.001; ns = non-significant.

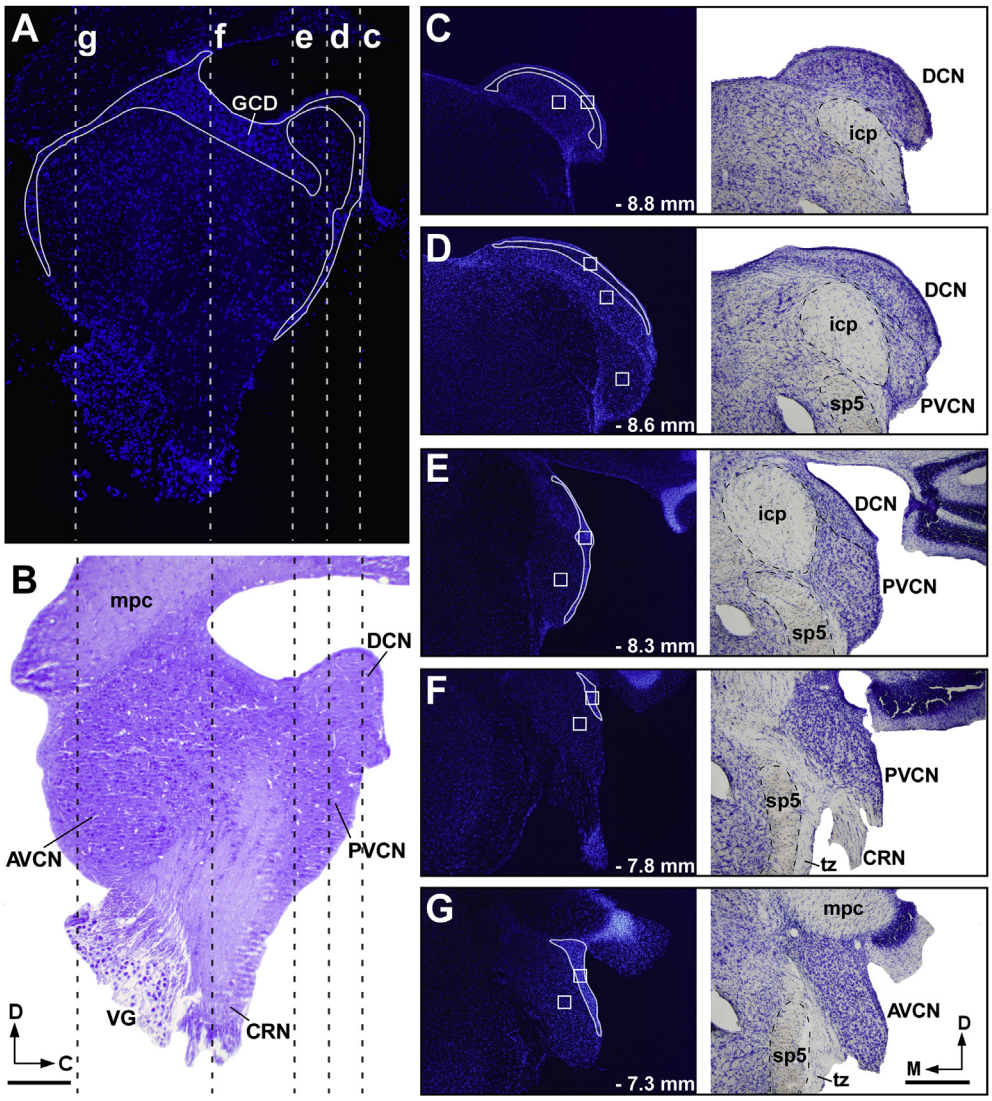

Fig. 8. Overview of the cochlear nucleus in the hamster and the slice planes used in this study. **A-B**. Sagittal sections of the hamster cochlear nucleus, stained with DAPI (A) and cresyl violet (B), show five representative levels (dashed lines) through the cochlear nucleus that were used for VGLUT2-immunoreactivity analysis. The GCD comprises the summed granular regions of the DCN layers, PVCN and AVCN. Notice the GCD outlined with a white line in A. **C-G.** Coronal sections corresponding to the slice planes depicted in A and B show representative locations where photomicrographs were taken for VGLUT2 analysis (indicated with squares in the DAPI stained sections). The regions of interest from caudal to rostral ends of cochlear nucleus, include the DCN (C, D and E), PVCN (D, E, and F), AVCN (G), and the granule cell domain (outlined with a white line in the DAPI stained sections). Each panel shows DAPI-stained sections and adjacent Nissl-staining sections, which allowed precise delineation of the cochlear nucleus subdivisions, and served as cytoarchitectural reference. The number at the bottom of each panel indicates the corresponding location in millimeters relative to Bregma. AVCN, anteroventral cochlear nucleus; CRN, cochlear root nucleus; DCN, dorsal cochlear nucleus; GCD, granule cell domain; icp, inferior cerebellar peduncle; mpc, middle cerebellar peduncle; PVCN, posteroventral cochlear nucleus; sp5, spinal trigeminal tract; tz, trapezoid body; VG, vestibular or Scarpa ganglion. Scale bars = 250 μm in A and B; 500 μm in C-G. (For interpretation of the references to color in this figure legend, the reader is referred to the Web version of this article).

magnocellular core of the PVCN and AVCN, whereas immunolabeling was sparser in the GCD (Fig. 10A). VGLUT2-immunolabeled puncta appeared to have a similar pattern and appearance in the DCN in both animal groups (Fig. 10A). In the cochlear root nucleus, we also observed qualitatively differences between control and GASH/Sal hamsters. VGLUT2-immunolabeling was also found in form of puncta surrounding dendrites and cell bodies of cochlear root neurons, with a much stronger immunolabeling in the GASH/Sal than in controls (Fig. 10B). In GASH/Sal animals, VGLUT2 immunohistochemistry gave so intense immunolabeling signal on the cell bodies of the cochlear root neurons that puncta were no clearly definable (Fig. 10B). In both animal groups, *en-passant* and mossy-like VGLUT2-immulabeled puncta were found outlining neuronal clusters in magnocellular regions of the ventral cochlear nucleus, preferentially in the AVCN (Fig. 10C). These neuronal clusters were identified as cells with ovoid shape, presumed to be bushy cells, with dendritic processes oriented toward adjacent cell bodies, which were frequently found next to each other (Fig. 10C). The observations based on qualitative assessment under light microscope were subjected to verification by a quantitative immunofluorescence analyses (Supplemental Material 3). Fig. 11A shows representative fluorescence microscopy images of all examined cochlear nucleus subdivisions and confirmed the altered distribution of VGLUT2-immunolabeling observed in the light microscopy analysis (for comparison see Figs. 9 and 11A). Quantitative immunofluorescence analysis showed that VGLUT2-puncta density was significantly increased in the PVCN and AVCN of the GASH/Sal as compared to controls ($p < 0.001$; Fig. 11B). By contrast, VGLUT2-

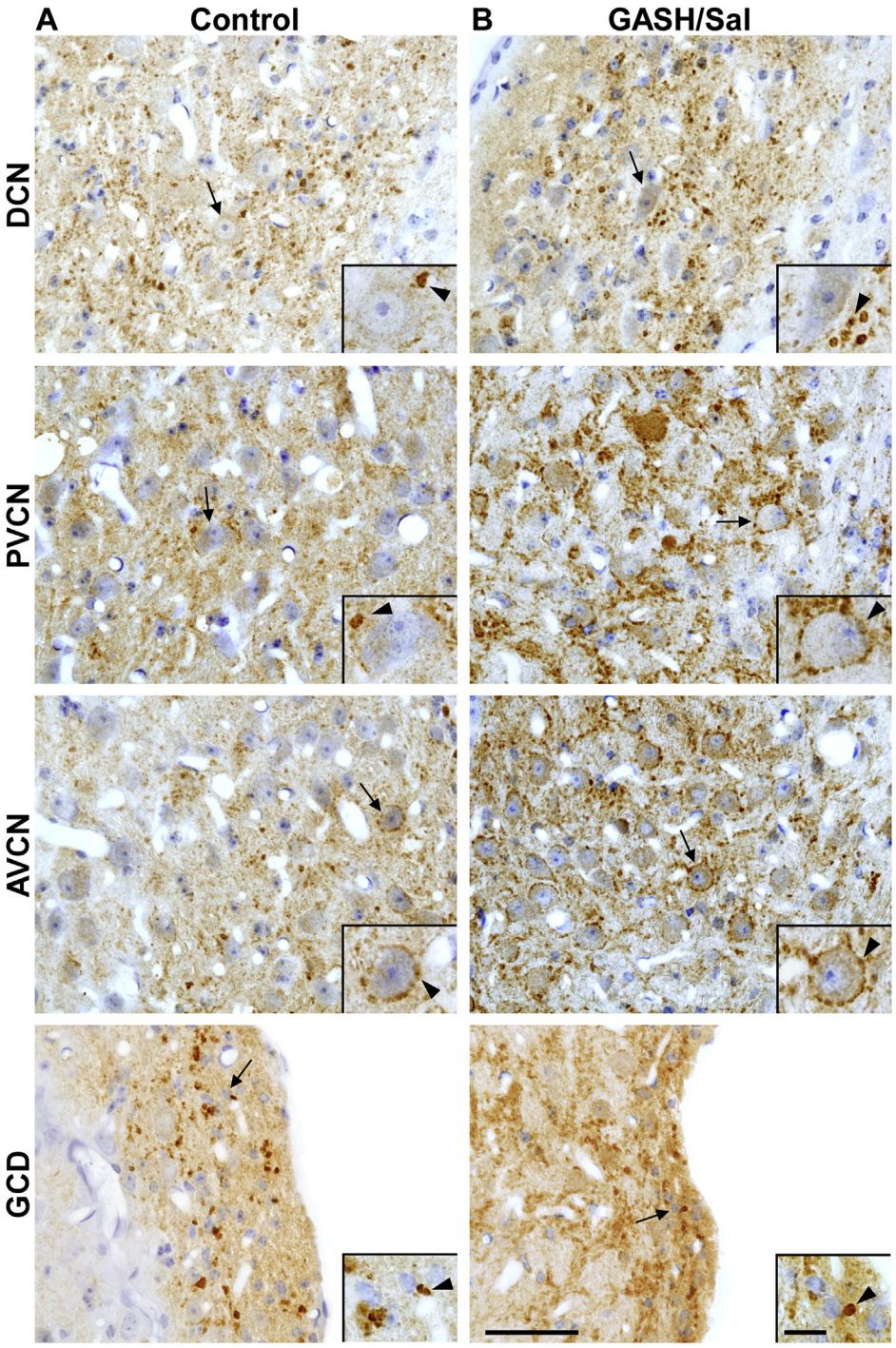

Fig. 9. VGLUT2-immunolabeling in the cochlear nucleus of the control (A) and GASH/Sal (B) hamsters. Light photomicrographs of 6-μm coronal sections counterstained with Carazzi's hematoxylin show VGLUT2-immunolabeling in the cochlear nucleus regions indicated in Fig. 8. The normal distribution pattern of VGLUT2-immunolabeling in the control animal (A) is characterized by moderate immunolabeling in the DCN, weak immunolabeling in the magnocellular cell areas of PVCN and AVCN, and intense immunolabeling in the granule cell domain. Note the qualitative differences of VGLUT2-immunolabeling in the GASH/Sal cochlear nucleus (B) compared to control hamsters (A). An evident increase in the VGLUT2-immunolabeling in the magnocellular cell areas of PVCN and AVCN of the GASH/Sal is observed in comparison to controls, whereas VGLUT2-immunolabeling in the GCD of the GASH/Sal is weakly immunolabeled. The insets show higher magnifications of VGLUT2-immunolabeled puncta (arrowheads) in close apposition to the cell bodies depicted with arrows in each panel. Notice the heterogeneity of the shape and size of VGLUT2-immunolabeled puncta in each of the cochlear nucleus subdivisions. AVCN, anteroventral cochlear nucleus; DCN, dorsal cochlear nucleus; GCD, granule cell domain; PVCN, posteroventral cochlear nucleus. Scale bars = 50 μm for all panels and 10 μm for insets.

puncta density was significantly reduced in the GCD of GASH/Sal animals ($p < 0.001$; Fig. 11B). No significant changes in the density of VGLUT2-immunolabeled puncta were seen in the DCN ($p < 0.001$; Fig. 11B). Differences in VGLUT2-puncta density across cochlear nucleus subdivisions of the GASH/Sal relative to control hamsters were highlighted as density ratios in Fig. 11C. VGLUT2 density were elevated above normal in the magnocellular areas of PVCN and AVCN as well as drastically reduced in GCD (Fig. 11C), suggesting an important reorganization of glutamatergic projections from auditory nerve and non-auditory sources to the

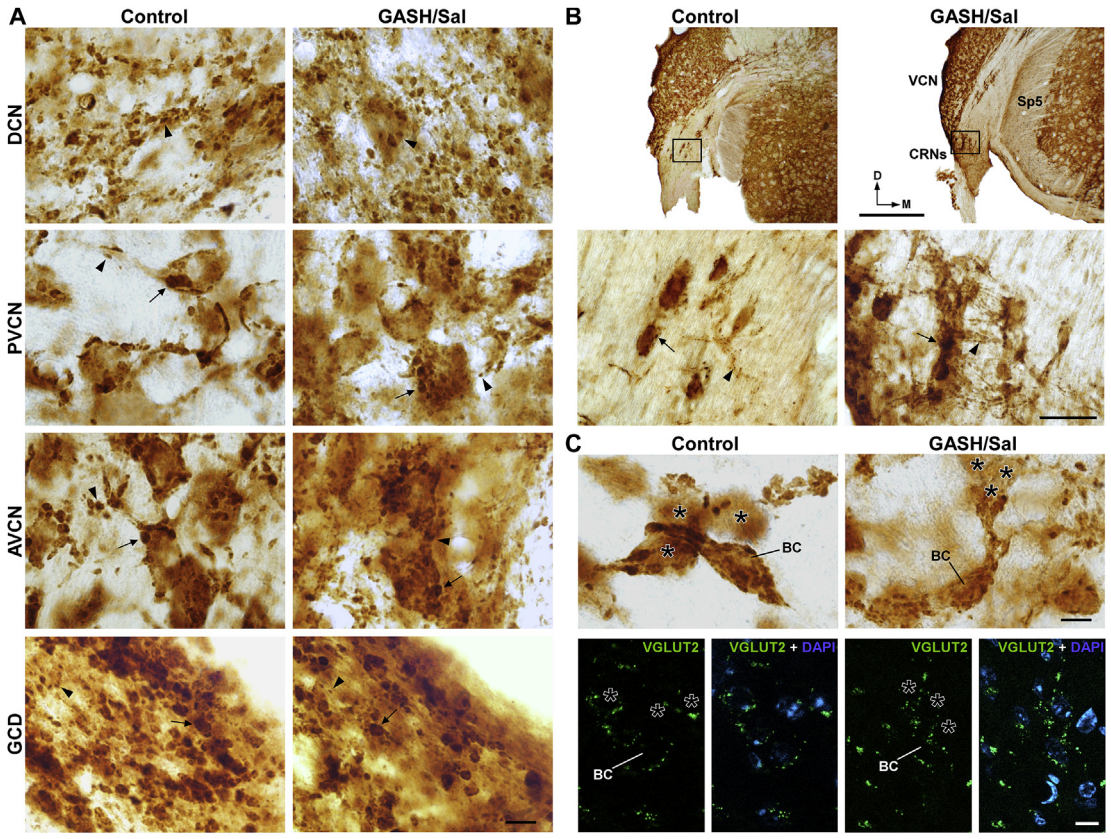

Fig. 10. Details of VGLUT2-immunolabeled puncta and neuronal clusters in the cochlear nucleus of the control and GASH/Sal hamsters. **A**. High magnification photomicrographs of 40-μm coronal sections show VGLUT2-immunolabeling in the cochlear nucleus regions indicated in Fig. 8. These sections correspond to the animals with ABR waveforms shown in Fig. 1. Notice the heterogeneity of the shape and size of VGLUT2-immunolabeled puncta in each of the cochlear nucleus subdivisions. Small-to medium-size *en-passant* endings (arrowheads) are observed in the deep layer of the DCN, magnocellular regions of the PVCN and AVCN as well as the GCD. Large VGLUT2-immunopositive mossy-like endings (arrows) are found in the magnocellular core of the PVCN and AVCN as well as the GCD. Notice that both *en-passant* (arrowheads) and mossy-like (arrows) endings decorated clusters of unlabeled cell somata and dendrites in magnocellular regions of the PVCN and AVCN. In comparison to controls, note that GASH/Sal animals had a very dense, patchy and disorganized VGLUT2-immunolabeling composed of varicosities in the magnocellular core of the PVCN and AVCN, whereas immunolabeling was sparser in the GCD. **B.** Low magnification photomicrographs of 40-μm coronal sections (upper panels) show VGLUT2-immunolabeling in the cochlear root nucleus of the control and GASH/Sal hamsters. Lower panels show high magnification photomicrographs corresponding to the frame depicted in the upper panels. Notice details of VGLUT2-immunolabeled puncta outlining unlabeled cell somata (arrows) and dendrites (arrowheads) of cochlear root neurons (CRNs). Also, note an increased number of VGLUT2 -immunolabeled puncta in the CRNs of the GASH/Sal compared to controls. **C**. VGLUT2-immunostaining shows that cells with ovoid shape, presumed to be bushy cells, form neuronal clusters in the AVCN of control and GASH/Sal hamsters. Upper panels show high magnification photomicrographs of VGLUT2-immunopositive puncta outlining a presumably bushy cell (BC) that oriented their dendrites towards adjacent neuronal somata (asterisks), which were frequently found next to each other. Lower panels show fluorescent microscopy images of VGLUT2-positive terminals (in green) distributed around unlabeled cell bodies and dendrites of adjacent bushy cells (asterisks). DAPI (in blue) was used for nuclear staining to show cell position. AVCN, anteroventral cochlear nucleus; BC, bushy cell; CRNs, cochlear root neurons; DCN, dorsal cochlear nucleus; GCD, granule cell domain; PVCN, posteroventral cochlear nucleus; VCN, ventral cochlear nucleus; sp5, spinal trigeminal tract. Scale bars = 10 μm for all panels in A and C; 500 μm for upper panels and 50 μm for lower panels in B. (For interpretation of the references to color in this figure legend, the reader is referred to the Web version of this article).

cochlear nucleus. Thus, cochlear nucleus regions in the GASH/Sal that should receive abundant auditory nerve terminals were dominated by non-auditory glutamatergic terminals, whereas regions preferentially innervated by non-auditory inputs reduce somatosensory cues. To determine whether this abnormal distribution of VGLUT2 inputs may lead to alterations in presynaptic glutamate release of cochlear nucleus efferents, we analyzed mRNA expression levels of *Vglut1* and *Vglut2* in the cochlear nucleus of the GASH/Sal. Cochlear nucleus tissue containing all the cochlear nucleus subdivisions were freshly dissected from control and GASH/Sal animals, and total RNA was extracted immediately. Quantitative gene expression data were normalized using β-actin as internal reference gene. Comparison of gene expression/β-actin ratios showed that gene expression of *Vglut1* and *Vglut2* in the GASH/Sal cochlear nucleus was significantly lower than in control animals ($p < 0.001$; Fig. 11D). These results indicated aberrant glutamatergic transmission in the flow of sound processing from the inner ear to the cochlear nucleus to the inferior colliculus.

4. Discussion

In the current study, we provided new morphological and molecular data of the auditory sensory epithelium and cochlear nucleus of the GASH/Sal and its counterpart wild-type Syrian golden hamster. We reported marked morphological alterations of the GASH/Sal cochlea as well as a significantly decreased mRNA expression of cochlear genes that correlate with drastically elevated auditory thresholds and reduced ABR wave I amplitudes. Despite preservation of IHCs and OHCs, the GASH/Sal exhibited a hearing loss that is displayed by specific cochlear abnormities such as disruption of the reticular lamina with severe disarray of stereocilliary tufts, a significant degeneration of SGNs as well as mild atrophy of the SV. These are manifestations of cochlear neuropathy that are compatible with auditory perceptual abnormalities and alterations in the auditory information processing and propagation. Indeed, our study also showed changes in the distribution of somatosensory VGLUT2 puncta as well as alteration of mRNA

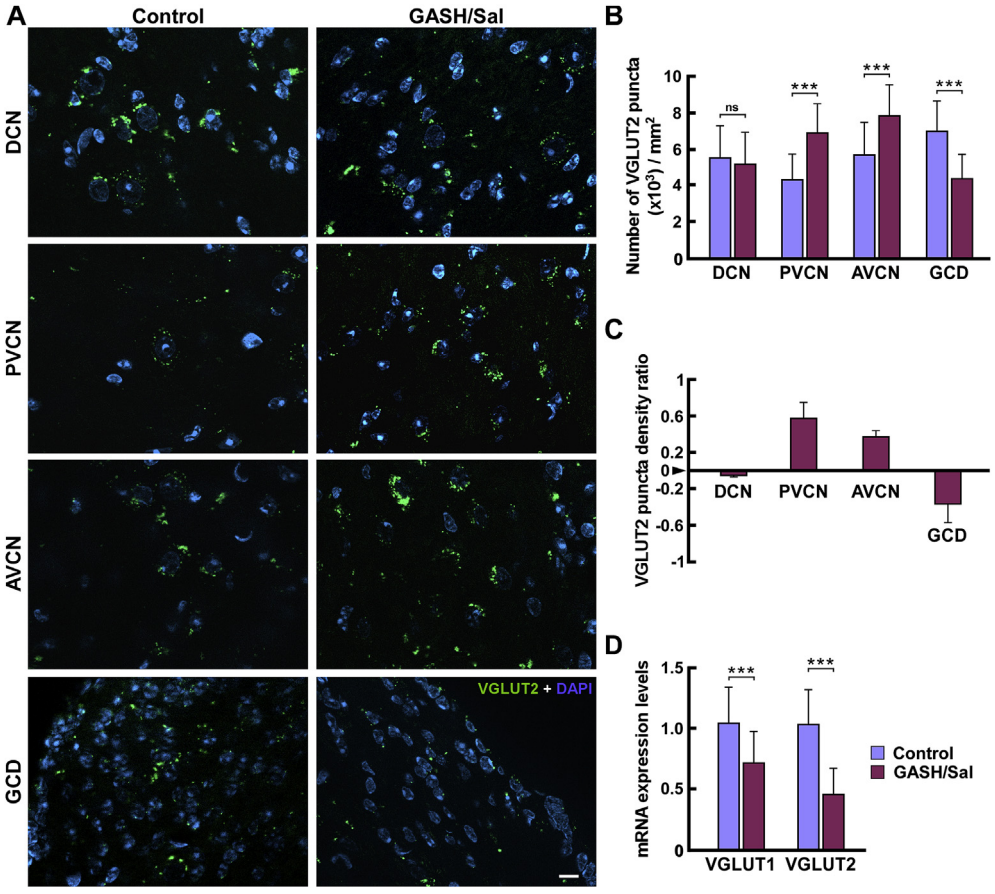

Fig. 11. Altered distribution of VGLUT2 axon terminals and mRNA expression of *Vglut1* and *Vglut2* genes in the cochlear nucleus of the GASH/Sal. **A.** Fluorescent microscopy images show VGLUT2-immunolabeled puncta (in green) across the cochlear nucleus subdivisions (depicted in Fig. 8) of control and GASH/Sal hamsters. DAPI (in blue) was used for nuclear staining to show cell position. Note the increase of VGLUT2 puncta in the PVCN and AVCN of the GASH/Sal compared to controls. Also, notice that VGLUT2 puncta are sparse in the GCD of the GASH/Sal. **B.** Histogram shows mean VGLUT2-puncta density (number of immunolabeled terminals per mm^2) in the cochlear nucleus subdivisions. VGLUT2-puncta densities are significantly increased in the magnocellular core of the PVCN and AVCN, but significantly decreased in the GCD of the GASH/Sal hamsters (compared to control hamsters). **C.** Plot shows the VGLUT2-puncta density ratio in the cochlear nucleus subdivisions of the GASH/Sal relative to controls, where 0 indicates no difference between GASH/Sal and control hamsters. Note VGLUT2 density is elevated above normal in the magnocellular core of the PVCN and AVCN as well as drastically reduced in GCD. Notice that DCN regions show normal VGLUT2 density values. **D.** Histogram shows relative quantities of transcripts of *Vglut1* and *Vglut2* genes in the cochlear nucleus of control and GASH/Sal animals. The relative mRNA expression of each gene was normalized to β-actin. ΔCt values were normalized to the average ΔCt of the cochlear nucleus tissues of control animals. For histograms B and D, controls are displayed in blue and GASH/Sal in purple. Each bar in the histograms is an average ± S.E.M. Asterisks indicate significance differences between control and GASH/Sal hamsters ("***" = p value ≤ 0.001; ns = non-significant). AVCN, anteroventral cochlear nucleus; DCN, dorsal cochlear nucleus; GCD, granule cell domain; PVCN, posteroventral cochlear nucleus. Scale bar = 10 μm for all panels in A. (For interpretation of the references to color in this figure legend, the reader is referred to the Web version of this article).

expression of *Vglut1* and *Vglut2* genes in the GASH/Sal cochlear nucleus. Together, these results indicated that the seizure-prone neural network of the GASH/Sal displays morphological and molecular abnormalities in the cochlea and cochlear nucleus, suggesting bottom-up modifications in glutamatergic transmission along the primary acoustic pathway, from the inner ear to the epileptogenic focus.

4.1. Methodological considerations: the wild-type golden hamster

The experimental design of the current study was based on comparisons with wild-type Syrian golden hamsters that were used as a control group. Thus, it was essential to characterize a strong control group that allow us to test the extent to which the morphological and molecular alterations are present in the GASH/Sal. The control hamsters used in our experiments exhibited an ABR waveform morphology as well as ABR thresholds, peak amplitudes and latencies in response to click stimuli very similar to those previously published (Church and Kaltenbach, 1993; Muñoz et al., 2017; Sánchez-Benito et al., 2017). Consistently with normal hearing function, our morphological study revealed normal appearance of the main cochlear structures, including the sensory hair cells in the organ of Corti, the SGNs and the stria vascularis. The anatomical developmental of the hamster cochlea has been studied extensively at light and electron microscopic level, but the data available in adult hamsters still remains incomplete (Pujol and Abonnenc, 1977; Simmons et al., 1991; Kaltenbach and Falzarano, 1994; Kaltenbach et al., 1994). At light microcopy, our morphometrically analyses of normal SGNs yielded similar, but slightly smaller, values in cell size than those previously reported for the golden hamster (Simmons et al., 1994; Fuentes-Santamaria et al., 2005). This difference might be explained due to variations in the total number of SGNs and regions of the spiral ganglion included in each study, possible shrinkage during the tissue processing, and whether or not type I and II SGNs were assessed together. As shown in rats (Berglund and Ryugo, 1986), the Nissl technique not only stained the entire population of SGNs, but also allowed us distinction and identification of type I and II neurons

based on their staining properties and different cell body size. However, our morphometric and quantification analyses were performed regardless of the neuron type as those cytological features were not clearly distinguishable in the GASH/Sal. Our study further quantifies the number of SGNs within the Rosenthal's canal, showing that densities per mm^3 were slightly higher in the golden hamster than in albino rats (Keithley and Feldman, 1979). Our morphological observations also indicated that the normal stria consisted of three layers of cells and a dense capillary network, with measures of SV thickness similar to those reported in other rodent species (Carlisle and Forge, 1989). At electron microcopy level, our analysis of the normal reticular lamina, including organization of hair cells, stereociliary bundles and supporting cochlear cells, as well as the measurements of stereocilia also coincides with previous reports (Kaltenbach and Falzarano, 1994; Kaltenbach et al., 1994). For the analysis of VGLUT2 puncta in the cochlear nucleus, it was necessary to determine the boundaries of the cochlear nucleus subdivisions based on histological characteristics. DCN, PVCN, AVCN and GCD were readily visible with Nissl and DAPI staining, and hence were considered separately in our analysis. These subdivisions in the cochlear nucleus hamster were also defined in other rodent species, in which similar relative volumes and basic structural features are found (Godfrey et al., 2016). Neither the reactivity of the VGLUT2 antibody used in our study nor the distribution of VGLUT2-immunolabeling in the cochlear nucleus subdivisions has been previously tested in the golden hamster. Our study provides several evidences that indicate this VGLUT2 antibody can be used as a marker of glutamatergic terminals in brain tissue of the golden hamster as efficiently as reported in other mammal species (Zhou et al., 2007; Gómez-Nieto and Rubio, 2009, 2011). First, the multiple sequence alignment showed that the specific target epitope is highly conserved for all VGLUT2 isoforms in the golden hamster. Second, the pattern of VGLUT2-immunolabeling in the cerebellar cortex of the hamster was consistent with that described in other rodent species (Hioki et al., 2003; Miyazaki et al., 2003). In addition, the distribution and morphology of VGLUT2 axon terminals in the hamster cochlear nucleus resembled to those reported in the guinea pig (Zhou et al., 2007), rat (Gómez-Nieto et al., 2009) and mouse (Heeringa et al., 2016). Finally, the VGLUT2-immunolabeled pattern in all regions of the hamster cochlear nucleus was consistently obtained using different cutting or immunodetection methods. Our immunostaining analysis in the hamster cochlear nucleus further showed VGLUT2 axon terminals outlining clusters of cell somata and dendrites in the magnocellular core of the PVCN and AVCN. These neuronal clusters resembled to those described in the ventral cochlear nucleus of the rat (Gómez-Nieto and Rubio, 2009) and monkey (Gómez-Nieto and Rubio, 2011), suggesting that a bushy cell network is also present in the hamster, and hence conserved across mammal species. It is also important to note in our comparative analysis that all control and GASH/Sal animals matched age, gender, housing, handling and care, therefore these characteristics can be ruled out as alternative explanations of any observed defects. Tissue samples for each set of experiments were obtained and processed in parallel for both animal groups, therefore the observed differences were not due to the passage of time, or any other experimental protocol variables such as incubation periods, temperature or sample manipulations. Our data analysis methods included single-blind assessments and quantification methods previously used by our research group (Gómez-Nieto et al., 2014; Sánchez-Benito et al., 2017), so experimental biases that arise from the observer effect were eliminated.

4.2. Morphological and molecular defects in the GASH/Sal cochlea: relevance to audiogenic seizure susceptibility

The inferior colliculus is considered the area of seizure initiation in rodent models of AGS susceptibility (Faingold et al., 1992; Garcia-Cairasco, 2002). This implies that the inferior colliculus is embedded in a web of pathologic connections that constitute a seizure-prone network to finally drive the AGS. Despite significant advances in understanding the seizure generation and propagation in the inferior colliculus (Garcia-Cairasco, 2002; N'Gouemo et al., 2009; Pinto et al., 2019), much less is known about the defects in lower auditory brainstem nuclei and the cochlea that might contribute to the seizure-prone network in AGS models. In this regard, recent studies from our research group reported that the GASH/Sal has an altered hearing sensitivity, showing high elevation of ABR thresholds and alterations in otoacoustic emissions (Muñoz et al., 2017; Sánchez-Benito et al., 2017). Our hearing evaluation of the GASH/Sal confirmed the increased hearing thresholds and further showed significant reductions of wave I and IV amplitudes, but normal latencies. The ABR wave I captures the synchronous firing of numerous auditory nerve fibers of the SGNs and wave IV is generated by the neuronal activity of the inferior colliculus (Church and Kaltenbach, 1993). Thus, our ABR results might be indicative of cochlear neuropathy, auditory nerve fiber reductions, decrease of synchronization of auditory nerve discharges and aberrant neuronal activity in the epileptogenic focus. The cochlear neuropathy, characterized by reduced ABR wave I amplitudes, is associated with damage at the cochlear synapse without loss of sensory hair cells and occurs after noise exposure, aging and may accompany several forms of hearing impairments, including tinnitus and hyperacusis (reviewed in Liberman and Kujawa, 2017; Milloy et al., 2017). Consistent with this, the cochlear histology of the GASH/Sal showed loss of SGNs and preservation of cochlear hair cells, indicating an auditory nerve deafferentation associated to a particular form of neuropathy that is no related with noise exposure. The normal or slightly elevated ABR waveforms II, III, and V in the GASH/Sal might reflect compensation mechanisms such as higher increased neural synchrony in central auditory regions. Something similar occurs in tinnitus, in which the normal wave V amplitude, despite a reduction in wave I, is evidence of an increased neural responsiveness in the central auditory system to compensate for the reduced activity of the auditory nerve (Schaette and McAlpine, 2011; Milloy et al., 2017). The normal latency of wave I in the GASH/Sal points to a defect in the receptor potential, instead of in the conduction velocities. Indeed, our electron microscopic study of the reticular lamina further showed marked disorganization of stereociliary tufts with loss, shortened or elongation of stereocilia. The compromised structure of the stereocilia bundle suggested an improper mechanoelectrical transduction in the GASH/Sal hair cells that correlates with the ABR results. In addition, the GASH/Sal exhibited disarray of regular arrangement in the cochlear hair cells, expansion of the surrounding supporting cochlear cells and blebs. Such abnormalities in the reticular lamina and stereocilia bundles were also observed in the GEPR rats (Penny et al., 1983) and BLSW mice (Charizopoulou et al., 2011), indicating that these cochlear defects are common among genetically AGS models, regardless of the animal species. Our study also revealed an important auditory hallmark of hearing impairment in the GASH/Sal that exhibited mild atrophy of the SV. Since strial dysfunction is associated to age-related hearing loss and alteration of cochlear homeostasis (Schuknecht et al., 1974; Gratton and Schulte, 1995; Patuzzi, 2011), the reduced SV thickness and fewer strial capillaries in the GASH/Sal might underlie the abnormalities of the organ of Corti and cause

important disturbances in sound transduction. Our molecular study further revealed concomitant molecular disruptions in the expression of cochlear genes that are involved in the mechanotransduction. The reduced mRNA levels of prestin in the GASH/Sal suggests loss of OHC electromotility, which in turn might affect cochlear amplification. Previous studies reported that absence of OHC electromotility in a prestin-knockout mice resulted in a loss of 40–60 dB in cochlear sensitivity (Liberman et al., 2002), and that uncoupling of hair-cell stereocilia from the tectorial membrane due to buckling of supporting cells may contribute for the loss of cochlear amplification (Flock et al., 1999; Nordmann et al., 2000). In line with that, our results showed that the GASH/Sal exhibited a greater than 40 dB cochlear sensitivity loss as well as defects of OHC stereocilia and alteration of Deiters' cells. The fact that the heads of Deiters' cells showed an increase of short microvilli might indicate that are sites of altered and intense metabolic exchange. Since Deiters' cells contribute to the micromechanics of the organ of Corti and to the control of hearing sensitivity (Laffon and Angelini, 1996; Flock et al., 1999), our results indicate that the surviving but dysfunctional package of OHCs and Deiters' cells in the GASH/Sal may negatively affect cochlear amplification. Interestingly, Penny et al. (1983) reported abnormal anatomical and functional associations of hair cells with the tectorial membrane in GEPR rats. It is noteworthy to highlight the similarity of the reticular lamina in both genetically AGS models. As occurs in GEPR rats (Penny et al., 1983), the hair cells of the GASH/Sal showed elongated stereocilia, non-parallel rows of OHCs as well as absence of normal "V-shaped" and "staircase" patterns of OHC stereocilia. The most plausible explanation is that the elongated and wavy stereocilia could represent a compensatory growth mechanism during development whereby hair cells attempt to contact the tectorial membrane for proper function (Penny et al., 1983). Normally, stereocilia growth during development requires actin polymerization to increase filament length that is precisely maintained during life by a slow turnover of actin at the apical tips (Narayanan et al., 2015). The elongation of stereocilia in the GASH/Sal therefore implies that the machinery for trafficking actin to the tips of stereocilia is still active, as being consistent with the presence of viable hair cells. It also suggests, however, an improper actin dynamics for controlling stereocilia length, which might negatively affect the normal mechanotransduction of the GASH/Sal hair cells. In addition, the signal transduction and role of the feedback mechanism in the sensitivity of the peripheral acoustic receptors might play a very important part of presumably pathological mechanisms of the AGS. In this regard, recent data from our laboratory has shown morphofunctional alterations in the olivocochlear efferent system of the GASH/Sal at naïve conditions, including absence of otoacoustic emissions in a wide range of frequencies and cell body shrinkage of olivocochlear neurons (Sánchez-Benito et al., 2017). Medial olivocochlear neurons innervate the OHCs modulating the cochlear amplifier gain (Warr and Beck, 1996; Cooper and Guinan, 2006; Gómez-Nieto et al., 2008a), therefore deficits in the olivocochlear efferent system of the GASH/Sal may contribute to an altered hearing sensitivity. Whether the molecular and morphological defects detected in the hair cells of the GASH/Sal were due to dysfunction of the olivocochlear efferent system, or vice versa, the olivocochlear neurons shrinkage were caused by an altered peripheral auditory system remains to be determined.

Our result showing decreased mRNA expression levels of *Cdh23 and Pcdh15* genes also supports the existence of an abnormal mechanotransduction in the GASH/Sal cochlea. Thus, mice with mutations in the two genes, *Cdh23* and *Pcdh15*, showed disruption of hair-bundle morphology and aberrant transducer currents in the sensory hair cells (Alagramam et al., 2011). As reported in those mouse mutants, our electron microscopy analysis showed similar structural alterations in the IHCs and OHCs, including loss of tip-links and disorganized hair bundles, suggesting an impaired cochlear transduction in the GASH/Sal. Interestingly, a case report has documented a patient harboring concomitant mutations in a DNA-repair gene (*PNKP*) and *Pcdh15* that caused early-onset seizures and congenital sensorineural hearing loss (Nakashima et al., 2014). As noted in this patient, GASH/Sal animals carry high-impact mutations in genes involved in DNA-repair processes (Díaz-Casado et al., 2020), and as our study shows, loss of *Pcdh15* mRNA expression that can be the result of genetic lesions. Given that partially shared phenotypes and underlying genetic alterations hint at a common disease, it is worthwhile to compare genetic variations and global patterns of gene expression (transcriptome) not only between different genetic AGS models (Damasceno et al., 2020), but also between human and model organisms with inherited propensity for developing seizures (Díaz-Casado et al., 2020).

An intriguing controversy that arise from our results is that the reduced mechanosensitivity in the GASH/Sal cochlea seems to be opposed to the hyperexcitability required for its AGS susceptibility. As definite possibility is that GASH/Sal animals have concomitant audiogenic susceptibility and age-related sensorineural hearing loss, wherein these two disease processes might course both dependently or independently of one another. If so, the relationship of these overlapping hearing pathologies with their corresponding molecular and morphofunctional correlates in the cochlea and auditory pathway might be not simple. As in other genetically AGS models, the innate susceptibility of the GASH/Sal to seizures appears and declines with age, so convulsions highly correlated with the development and decline of auditory function (Henry,1985; Misawa et al., 2002; Charizopoulou et al., 2011; Muñoz et al., 2017). Early studies in genetically AGS mice and primed AGS models with elevated high frequency thresholds support that susceptibility is associated to a certain degree of high frequency dysfunction or damage during cochlear development (Henry, 1985; Henry and Buzonne, 1986). Furthermore, it has been suggested that AGS susceptibility after acoustic trauma in neonatal rats depend on derangements of topographic frequency representation in the inferior colliculus, which were probably due to abnormal tonotopic development of the cochlea (Pierson and Snyder-Keller, 1994; Garcia-Cairasco, 2002). Our electron microscopy results showing that changes in the GASH/Sal cochlea were more pronounced in the basal (high frequency) regions argued in favor of this hypothesis, but not the uniform loss of SGNs in all three regions of the cochlea. Studies in genetically AGS mice with specific mutations in cochlear genes further revealed that age-related hearing loss does not significantly contribute to the AGS susceptibility or the developmental regulation of seizures, suggesting that these two pathologies are independent (Misawa et al., 2002; Charizopoulou et al., 2011). With the advent of new molecular tools applied to the characterization of seizure susceptibility in genetically rodent strains (Bosque et al., 2019), a longitudinally study showing a correlation between the cochlear dysfunction causing upstream excitability and the sound-triggered seizures during the GASH/Sal lifespan might clarify the complex relationship between its sensorineural hearing loss and its AGS susceptibility.

4.3. Altered glutamate release in the GASH/Sal cochlear nucleus: relevance to audiogenic seizure susceptibility

Along with the molecular and morphological alterations in the organ of Corti and consistent with the loss of SGNs and auditory nerve deafferentation, our RT-qPCR analysis showed a reduction of *Vglut1* and *Vglut2* gene expression levels in the GASH/Sal cochlea. VGLUT1 and VGLUT2 are commonly used as markers for glutamate

release (Takamori, 2006) and are expressed in the SGNs, but not in the cochlear hair cells (Seal et al., 2008). Since type I auditory nerve fibers are the major source of excitation to the cochlear nucleus (Lorente de Nó, 1981), our results imply a decrease in glutamate concentrations in the GASH/Sal cochlear nucleus. However, apart from the primary auditory afferents, the cochlear nucleus receives glutamatergic inputs that are from intrinsic (i.e. parallel fibers from the granule cells) as well as other extrinsic sources (i.e. mossy fibers from somatosensory origin) (reviewed in Rubio, 2019). Then the question becomes, what are the effects of cochlear abnormalities on the glutamatergic signaling of the GASH/Sal cochlear nucleus? In an attempt to answer this question, our study determined the distribution of VGLUT2 puncta in all cochlear nucleus regions. In the cochlear nucleus, VGLUT1 is preferentially associated with auditory nerve terminals and VGLUT2 with non-auditory (somatosensory) terminals (Zhou et al., 2007; Gómez-Nieto and Rubio, 2009). In the GASH/Sal, our immunostaining results showed increases of VGLUT2 density in the magnocellular core of the PVCN and AVCN as compared to controls. PVCN and AVCN represents the beginning of the binaural pathway through its projections to the superior olivary complex as well as the monaural pathway through direct projections to the inferior colliculus, conveying the incoming signals from the cochlear afferents in an accurate and timely manner (Oliver et al., 1999; reviewed in Malmierca, 2003). Thus, the increased VGLUT2-puncta density in the PVCN and AVCN of the GASH/Sal, possibly derived from somatosensory projections to the cochlear nucleus, might be a compensatory mechanism to solve lack of glutamatergic input from the auditory nerve, but in turn might contribute to aberrant neural activity in the inferior colliculus. In support of this argument, it has been suggested that divergent multiple-contact synapses of cochlear and non-cochlear inputs on bushy cells' clusters underlie the morphological substrate for the enhanced synchronization of bushy cells firing (Gómez-Nieto and Rubio, 2009). Therefore, a higher number of VGLUT2 puncta in the bushy cell network of the GASH/Sal might adversely affect the output signal of the ventral cochlear nucleus. In addition, elevated spontaneous rates in neurons of the ventral cochlear nucleus, in compensatory response to deafening, were correlated to the hyperactivity developed in the inferior colliculus after cochlear trauma (Vogler et al., 2011). The results of this study, along with others, suggested that tinnitus and hyperacusis are associated with cochlear deafferentation or neuropathy as well as elevated hyperactivity, enhanced synchrony and altered balance between auditory nerve and somatosensory inputs in the ventral cochlear nucleus (Zeng et al., 2009; Vogler et al., 2011; Liberman and Kujawa, 2017; Heeringa et al., 2018). Whether these perceptual abnormalities are also present in the GASH/Sal remains to be elucidated. On the other hand, our study indicated the opposite VGLUT2-immunolabeled pattern in the GCD, showing a reduced density of VGLUT2 puncta in GASH/Sal animals as compared to controls. The GCD is not a major target of type I auditory nerve fibers, but on the contrary receives type II auditory nerve inputs as well as a variety of descending auditory inputs and non-auditory projections from somatosensory nuclei (Malmierca, 2003; Rubio, 2019). This unique set of afferent projections might explain the opposed results in VGLUT2 densities between the GCD and the magnocellular regions in the GASH/Sal. Remarkably, changes in VGLUT1 and VGLUT2-immunoreactivity were also reported in the cochlear nucleus after cochlear damage by intracochlear injections of kanamycin (Zeng et al., 2009). Zeng et al. (2009) showed reductions in VGLUT1-immunoreactivity in magnocellular regions of the cochlear nucleus and increases in VGLUT2-immunoreactivity in all regions of the cochlear nucleus, particularly those that received non-auditory inputs as the GCD (Heeringa et al., 2016). This altered VGLUT2-immunolabeleing pattern after cochlear deafferentation is partially at odds with those observed in the GASH/Sal, suggesting that the plasticity of somatosensory inputs to the GASH/Sal cochlear nucleus could be associated to audiogenic susceptibility rather than being mere correlates of cochlear deafferentation. In fact, the deep and fusiform cell layer of the DCN in control and GASH/Sal animals showed no significant differences in VGLUT2 density, while VGLUT2-immunoreactivity in those regions of the DCN were affected after the cochlear damage (Zeng et al., 2009). The DCN is the principal part of the monaural pathway to the central nucleus of the inferior colliculus (Oliver et al., 1999) and its glutamatergic afferent innervation also differs from other cochlear nucleus regions, including projections from a great variety of auditory and non-auditory sources (Malmierca, 2003; Rubio, 2019). Thus, our results indicated that the structural and molecular abnormalities in the GASH/Sal cochlea had differently effects on the glutamatergic system of each cochlear nucleus subdivisions, and hence the bottom-up pathways to the inferior colliculus might be affected in different degrees. In agreement with this hypothesis, our finding showing lower mRNA transcript levels of *Vglut1* and *Vglut2* in the cochlear nucleus suggests a presynaptic dysregulation of glutamate release in the inferior colliculus of the GASH/Sal. VGLUT1 and VGLUT2 differentiate complementary patterns of glutamatergic inputs into the inferior colliculus with VGLUT1 endings predominantly on the dendrites and VGLUT2 on both dendrites and somas (Altschuler et al., 2008). Since those neurons with flattened dendritic arbors constitutes the structural basis for the tonotopic organization of the inferior colliculus (Malmierca, 2003), the glutamate pathology derived from the GASH/Sal cochlear nucleus might affect a number of pre- and postsynaptic events in the inferior colliculus, that finally might be reflected in a tonotopic map disruption or hyperexcitability. In this regard, studies that mapped Fos-immunoreactivity in the inferior colliculus of AGS rodent models of genetic origin and after priming procedures (neonatal acoustic trauma) provided clear evidences that the deteriorations in tonotopic organization of the inferior colliculi underlie AGS susceptibility (Pierson and Snyder-Kelly, 1994; Klein et al., 2004). Glutamate receptors are also involved in AGS networks of the inferior colliculus, in which the mechanisms of initiation and propagation of seizures are differently controlled by different types of ionotropic glutamate receptors (Yasuda et al., 2000). Thus, presynaptic dysregulation of glutamate release in the GASH/Sal inferior colliculus might lead to postsynaptic strengthening or weakening of synapsis via changes in glutamate receptors, and that could eventually culminate in long-term changes in the seizure-free prone neural circuitry. Supporting this, recent physiological and behavioural experiments demonstrated that corruption of the neural synchronization in the inferior colliculus is involved in the AGS susceptibility of the WAR model under seizure-free conditions (Pinto et al., 2019). Future experiments are required to provide a clear picture of the role of the glutamate system in triggering shift in connectivity and synchronicity that contributes to ictogenesis in the inferior colliculus of the GASH/Sal.

5. Concluding remarks

The present work examined the morphofunctional and molecular abnormalities of the cochlea and cochlear nucleus in the genetically audiogenic seizure-prone hamster GASH/Sal by comparison to control animals. In the Syrian golden hamster, the ABR waveforms, the reticular lamina, the cochlear gene expression profiles as well as the VGLUT2-immunolabeling pattern and anatomical characteristics of the cochlear nucleus subdivisions are equivalent to other rodent species. As compared to the wild-type golden hamster, the cochlear histopathology of the GASH/Sal

showed preservation of the sensory hair cells, but a significant loss of SGNs and mild atrophy of the SV in all cochlear turns. At the electron microscopy level, the reticular lamina of the GASH/Sal exhibited disarray of stereociliary tufts, blebs, and elongated stereocilia in the IHCs and OHCs. Loss of stereocilia tufts and tip-links in the OHCs were particularly more pronounced in the basal turn of the cochlea and caused absence of the normal bundle morphology. Non-parallel rows of OHCs were also detected, presumably due to distention of the Deiters' cells. Consistently with those morphological manifestations, the GASH/Sal cochlea showed abnormal gene expression patterns of *prestin*, *Cdh23*, *Pcdh15*, *Vglut1* and *Vglut2*, suggesting that the mechanotransduction mechanism in the sensory hair cells is markedly altered. All these morphological and molecular defects in the GASH/Sal cochlea correlated to ABR waveform I alterations and elevated auditory thresholds. Crucially, these findings indicated that the GASH/Sal has a complex hearing impairment with severe hearing loss and cochlear neuropathy, in which acoustic cues are not faithfully transmitted from the inner ear to the cochlear nucleus. In fact, the distribution of VGLUT2 axon terminals was differently affected in each cochlear nucleus subdivision of the GASH/Sal. A significant increase in VGLUT2-puncta density were found in magnocellular regions of the PVCN and AVCN, whereas a drastic reduction was observed in the GCD. The deep and fusiform cell layer of the GASH/Sal DCN were unaffected. These results indicated a reorganization of glutamatergic projections from non-auditory sources to the GASH/Sal cochlear nucleus, which could be a compensatory mechanism of the cochlear neuropathy, but in turn contributes to either desynchronization or enhanced synchrony of cochlear nucleus neurons. In correlation with this finding, our molecular study showed a disruption in the gene expression of *Vglut1* and *Vglut2* in the GASH/Sal cochlear nucleus, suggesting aberrant glutamatergic release in the epileptogenic focus. Since our experiments were conducted in a genetically AGS model under seizure-free conditions, the alterations at the morphological and molecular connectome level of the primary acoustic pathway form part of the GASH/Sal seizure-prone neural network and represent the manifestations of genetic and developmental defects of its seizure susceptibility.

Declaration of competing interest

The authors declare no competing interests.

CRediT authorship contribution statement

David Sánchez-Benito: Conceptualization, Formal analysis, Investigation, Visualization, Validation, Writing - review & editing. **Miguel A. Hyppolito:** Investigation, Writing - review & editing. **Antonio J. Alvarez-Morujo:** Investigation, Writing - review & editing. **Dolores E. López:** Conceptualization, Formal analysis, Project administration, Funding acquisition, Supervision, Writing - review & editing. **Ricardo Gómez-Nieto:** Writing - original draft, Conceptualization, Methodology, Formal analysis, Investigation, Visualization, Validation, Project administration, Funding acquisition, Supervision, Writing - review & editing.

Acknowledgement

The authors wish to thank Rosa García Aparicio, Adriana Murashima, *Elena Díaz-Casado*, *Marianny Pernia* and Samara Damasceno for excellent technical assistance. We thank Daniel Medeiros for providing the MATLAB script. This study was supported by a research grant from the Instituto de Salud Carlos III (ISCIII), co-financed with European Union FEDER funds (#PI19/01364, PIs: Dolores E. López and Ricardo Gómez-Nieto), the Regional Government of Castilla y León (#SA070P17; PI: Dolores E. López) and the research fellowship grant (#EDU/346/2013; awarded to David Sánchez-Benito). We also thank the International Collaboration Agreement between the FAPESP and the University of Salamanca (#2019/16574–2; PIs: Dolores E. López and Norberto Garcia-Cairasco).

Appendix A. Supplementary data

Supplementary data to this article can be found online at https://doi.org/10.1016/j.heares.2020.107973.

References

Abercrombie, M., 1946. Estimation of nuclear population from microtome sections. Anat. Rec. 94, 239–247. https://doi.org/10.1002/ar.1090940210.

Alagramam, K.N., Goodyear, R.J., Geng, R., Furness, D.N., van Aken, A.F., Marcotti, W., Kros, C.J., Richardson, G.P., 2011. Mutations in protocadherin 15 and cadherin 23 affect tip links and mechanotransduction in mammalian sensory hair cells. PLoS One 6 (4), e19183. https://doi.org/10.1371/journal.pone.0019183.

Altschuler, R.A., Tong, L., Holt, A.G., Oliver, D.L., 2008. Immunolocalization of vesicular glutamate transporters 1 and 2 in the rat inferior colliculus. Neuroscience 154 (1), 226–232. https://doi.org/10.1016/j.neuroscience.2008.03.036.

Barrera-Bailón, B., Oliveira, J.A.C., López, D.E., Muñoz de la Pascua, L.J., Garcia-Cairasco, N., Sancho, C., 2013. Pharmacological and neuroethological study of three antiepileptic drugs in the genetic audiogenic seizure hamster (GASH:Sal). Epilepsy Behav. 28 (3), 413–425. https://doi.org/10.1016/j.yebeh.2013.05.028.

Barrera-Bailón, B., Oliveira, J.A.C., López, D.E., Muñoz, L.J., Garcia-Cairasco, N., Sancho, C., 2017. Pharmacological and neuroethological study of the acute and chronic effects of lamotrigine in the genetic audiogenic seizure hamster (GASH:Sal). Epilepsy Behav. 71 (Pt B), 207–217. https://doi.org/10.1016/j.yebeh.2015.11.005.

Berglund, A.M., Ryugo, D.K., 1986. A monoclonal antibody labels type II neurons of the spiral ganglion. Brain Res. 383 (1–2), 327–332. https://doi.org/10.1016/0006-8993(86)90034-X.

Berglund, A.M., Ryugo, D.K., 1991. Neurofilament antibodies and spiral ganglion neurons of the mammalian cochlea. J. Comp. Neurol. 306 (3), 393–408. https://doi.org/10.1002/cne.903060304, 1991 Apr 15.

Bosque, J.R., Gómez-Nieto, R., Hormigo, S., Herrero-Turrión, M.J., Díaz-Casado, E., Sancho, C., López, D.E., 2019. Molecular tools for the characterization of seizure susceptibility in genetic rodent models of epilepsy. Epilepsy Behav. 1, 106594. https://doi.org/10.1016/j.yebeh.2019.106594.

Browning, R.A., 1986. Neuroanatomical localization of structures responsible for seizures in the GEPR: lesion studies. Life Sci. 39 (10), 857–867. https://doi.org/10.1016/0024-3205(86)90367-X.

Carballosa-Gonzalez, M.M., Muñoz, L.J., López-Alburquerque, T., Pardal-Fernández, J.M., Nava, E., de Cabo, C., Sancho, C., López, D.E., 2013. EEG characterization of audiogenic seizures in the hamster strain GASH:Sal. Epilepsy Res. 106 (3), 318–325. https://doi.org/10.1016/j.eplepsyres.2013.07.001.

Carlisle, L., Forge, A., 1989. The vessels of the stria vascularis: quantitative comparison of three rodent species. Hear. Res. 38 (1–2), 111–117. https://doi.org/10.1016/0378-5955(89)90132-9.

Charizopoulou, N., Lelli, A., Schraders, M., Ray, K., Hildebrand, M.S., Ramesh, A., Srisailapathy, C.R., Oostrik, J., Admiraal, R.J., Neely, H.R., Latoche, J.R., Smith, R.J., Northup, J.K., Kremer, H., Holt, J.R., Noben-Trauth, K., 2011. Gipc3 mutations associated with audiogenic seizures and sensorineural hearing loss in mouse and human. Nat. Commun. 2, 201. https://doi.org/10.1038/ncomms1200.

Church, M.W., Kaltenbach, J.A., 1993. The hamster's auditory brain stem response as a function of stimulus intensity, tone burst frequency, and hearing loss. Ear Hear. 14 (4), 249–257. https://doi.org/10.1097/00003446-199308000-00004.

Colmenárez-Raga, A.C., Díaz, I., Pernia, M., Pérez-González, D., Delgado-García, J.M., Carro, J., Plaza, I., Merchán, M.A., 2019. Reversible functional changes evoked by anodal epidural direct current electrical stimulation of the rat auditory cortex. Front. Neurosci. 13, 356. https://doi.org/10.3389/fnins.2019.00356.

Cooper, N.P., Guinan Jr., J.J., 2006. Efferent-mediated control of basilar membrane motion. J. Physiol. 576 (Pt 1), 49–54. https://doi.org/10.1113/jphysiol.2006.114991.

Damasceno, S., Gómez-Nieto, R., Garcia-Cairasco, N., Herrero-Turrión, M.J., Marín, F., Lopéz, D.E., 2020. Top common differentially expressed genes in the epileptogenic nucleus of two strains of rodents susceptible to audiogenic seizures: WAR and GASH/sal. Front. Neurol. 11, 33. https://doi.org/10.3389/fneur.2020.00033.

De Sarro, G., Russo, E., Citraro, R., Meldrum, B.S., 2017. Genetically epilepsy-prone rats (GEPRs) and DBA/2 mice: two animal models of audiogenic reflex epilepsy for the evaluation of new generation AEDs. Epilepsy Behav. 71 (Pt B), 165–173. https://doi.org/10.1016/j.yebeh.2015.06.030.

Díaz-Casado, E., Gómez-Nieto, R., Pereda, J.M., Muñoz, L.J., Jara, M., López, D.E., 2020. Analysis of gene variants in the GASH/Sal model of epilepsy. PLoS ONE 15 (3), e0229953. https://doi.org/10.1371/journal.pone.0229953.

Doretto, M.C., Fonseca, C.G., Lóbo, R.B., Terra, V.C., Oliveira, J.A., Garcia-Cairasco, N., 2003. Quantitative study of the response to genetic selection of the Wistar

audiogenic rat strain (WAR). Behav. Genet. 33 (1), 33–42. https://doi.org/10.1023/a:1021099432759.
Faingold, C.L., Naritoku, D.K., Copley, C.A., Randall, M.E., Riaz, A., Anderson, C.A., Arnerić, S.P., 1992. Glutamate in the inferior colliculus plays a critical role in audiogenic seizure initiation. Epilepsy Res. 13 (2), 95–105. https://doi.org/10.1016/0920-1211(92)90064-Z.
Flock, A., Flock, B., Fridberger, A., Scarfone, E., Ulfendahl, M., 1999. Supporting cells contribute to control of hearing sensitivity. J. Neurosci. 19 (11), 4498–4507. https://doi.org/10.1523/JNEUROSCI.19-11-04498.1999.
Fremeau Jr., R.T., Troyer, M.D., Pahner, I., Nygaard, G.O., Tran, C.H., Reimer, R.J., Bellocchio, E.E., Fortin, D., Storm-Mathisen, J., Edwards, R.H., 2001. The expression of vesicular glutamate transporters defines two classes of excitatory synapse. Neuron 31 (2), 247–260. https://doi.org/10.1016/s0896-6273(01)00344-0.
Fuentes-Santamaría, V., Cantos, R., Alvarado, J.C., García-Atarés, N., López, D.E., 2005. Morphologic and neurochemical abnormalities in the auditory brainstem of the genetically epilepsy-prone hamster (GPG/Vall). Epilepsia 46 (7), 1027–1045. https://doi.org/10.1111/j.1528-1167.2005.68104.x.
Furness, D.N., Lawton, D.M., 2003. Comparative distribution of glutamate transporters and receptors in relation to afferent innervation density in the mammalian cochlea. J. Neurosci. 23 (36), 11296–11304. https://doi.org/10.1523/JNEUROSCI.23-36-11296.2003. In press.
García-Cairasco, N., 2002. A critical review on the participation of inferior colliculus in acoustic-motor and acoustic-limbic networks involved in the expression of acute and kindled audiogenic seizures. Hear. Res. 168 (1–2), 208–222. https://doi.org/10.1016/s0378-5955(02)00371-4, 2002 Jun.
Godfrey, D.A., Lee, A.C., Hamilton, W.D., Benjamin 3rd, L.C., Vishwanath, S., Simo, H., Godfrey, L.M., Mustapha, A.I., Heffner, R.S., 2016. Volumes of cochlear nucleus regions in rodents. Hear. Res. 339, 161–174. https://doi.org/10.1016/j.heares.2016.07.003.
Gómez-Nieto, R., Rubio, M.E., López, D.E., 2008a. Cholinergic input from the ventral nucleus of the trapezoid body to cochlear root neurons in rats. J. Comp. Neurol. 506 (3), 452–468. https://doi.org/10.1002/cne.21554.
Gómez-Nieto, R., Horta-Junior, J.A., Castellano, O., Herrero-Turrión, M.J., Rubio, M.E., López, D.E., 2008b. Neurochemistry of the afferents to the rat cochlear root nucleus: possible synaptic modulation of the acoustic startle. Neuroscience 154 (1), 51–64. https://doi.org/10.1016/j.neuroscience.2008.01.079.
Gómez-Nieto, R., Rubio, M.E., 2009. A bushy cell network in the rat ventral cochlear nucleus. J. Comp. Neurol. 516 (4), 241–263. https://doi.org/10.1002/cne.22139.
Gómez-Nieto, R., Rubio, M.E., 2011. Ultrastructure, synaptic organization, and molecular components of bushy cell networks in the anteroventral cochlear nucleus of the rhesus monkey. Neuroscience 179, 188–207. https://doi.org/10.1016/j.neuroscience.2011.01.058.
Gómez-Nieto, R., Horta-Júnior, J.de A., Castellano, O., Millian-Morell, L., Rubio, M.E., López, D.E., 2014. Origin and function of short-latency inputs to the neural substrates underlying the acoustic startle reflex. Front. Neurosci. 8, 216. https://doi.org/10.3389/fnins.2014.00216.
Gratton, M.A., Schulte, B.A., 1995. Alterations in microvasculature are associated with atrophy of the stria vascularis in quiet-aged gerbils. Hear. Res. 82, 44–52. https://doi.org/10.1016/0378-5955(94)00161-I.
Grone, B.P., Baraban, S.C., 2015. Animal models in epilepsy research: legacies and new directions. Nat. Neurosci. 18 (3), 339–343. https://doi.org/10.1038/nn.3934.
Heeringa, A.N., Stefanescu, R.A., Raphael, Y., Shore, S.E., 2016. Altered vesicular glutamate transporter distributions in the mouse cochlear nucleus following cochlear insult. Neuroscience 315, 114–124. https://doi.org/10.1016/j.neuroscience.2015.12.009.
Heeringa, A.N., Wu, C., Chung, C., West, M., Martel, D., Liberman, L., Liberman, M.C., Shore, S.E., 2018. Glutamatergic projections to the cochlear nucleus are redistributed in tinnitus. Neuroscience 391, 91–103. https://doi.org/10.1016/j.neuroscience.2018.09.008.
Henry, K.R., 1985. Cochlear function and audiogenic seizures: developmental covariance in the LP/J mouse. Dev. Psychobiol. 18 (6), 461–466. https://doi.org/10.1002/dev.420180603.
Henry, K.R., Buzzone, R., 1986. Auditory physiology and behavior in RB/1bg, RB/3bg, and their F1 hybrid mice (Mus musculus): influence of genetics, age, and acoustic variables on audiogenic seizure thresholds and cochlear functions. J. Comp. Psychol. 100 (1), 46–51. https://doi.org/10.1037/0735-7036.100.1.46.
Hioki, H., Fujiyama, F., Taki, K., Tomioka, R., Furuta, T., Tamamaki, N., Kaneko, T., 2003. Differential distribution of vesicular glutamate transporters in the rat cerebellar cortex. Neuroscience 117 (1), 1–6. https://doi.org/10.1016/s0306-4522(02)00943-0.
Kaltenbach, J.A., Falzarano, P.R., 1994. Postnatal development of the hamster cochlea. I. Growth of hair cells and the organ of Corti. J. Comp. Neurol. 340 (1), 87–97. https://doi.org/10.1002/cne.903400107.
Kaltenbach, J.A., Falzarano, P.R., Simpson, T.H., 1994. Postnatal development of the hamster cochlea. II. Growth and differentiation of stereocilia bundles. J. Comp. Neurol. 350 (2), 187–198. https://doi.org/10.1002/cne.903500204.
Kandratavicius, L., Balista, P.A., Lopes-Aguiar, C., Ruggiero, R.N., Umeoka, E.H., Garcia-Cairasco, N., Bueno-Junior, L.S., Leite, J.P., 2014. Animal models of epilepsy: use and limitations. Neuropsychiatric Dis. Treat. 10, 1693–1705. https://doi.org/10.2147/NDT.S50371.
Kazmierczak, P., Sakaguchi, H., Tokita, J., Wilson-Kubalek, E.M., Milligan, R.A., Müller, U., Kachar, B., 2007. Cadherin 23 and protocadherin 15 interact to form tip-link filaments in sensory hair cells. Nature 449 (7158), 87–91. https://doi.org/10.1038/nature06091, 2007 Sep. 6.
Keithley, E.M., Feldman, M.L., 1979. Spiral ganglion cell counts in an age-graded series of rat cochleas. J. Comp. Neurol. 188 (3), 429–442. https://doi.org/10.1002/cne.901880306, 1979 Dec 1.
Keithley, E.M., Canto, C., Zheng, Q.Y., Wang, X., Fischel-Ghodsian, N., Johnson, K.R., 2005. Cu/Zn superoxide dismutase and age-related hearing loss. Hear. Res. 209 (1–2), 76–85. https://doi.org/10.1016/j.heares.2005.06.009, 2005 Nov.
Klein, B.D., Fu, Y.H., Ptacek, L.J., White, H.S., 2004. c-Fos immunohistochemical mapping of the audiogenic seizure network and tonotopic neuronal hyperexcitability in the inferior colliculus of the Frings mouse. Epilepsy Res. 62 (1), 13–25. https://doi.org/10.1016/j.eplepsyres.2004.06.007.
Laffon, E., Angelini, E., 1996. On the Deiters cell contribution to the micromechanics of the organ of Corti. Hear. Res. 99 (1–2), 106–109. https://doi.org/10.1016/s0378-5955(96)00089-5.
Liberman, M.C., Gao, J., He, D.Z., Wu, X., Jia, S., Zuo, J., 2002. Prestin is required for electromotility of the outer hair cell and for the cochlear amplifier. Nature 419 (6904), 300–304. https://doi.org/10.1038/nature01059.
Liberman, M.C., Kujawa, S.G., 2017. Cochlear synaptopathy in acquired sensorineural hearing loss: manifestations and mechanisms. Hear. Res. 349, 138–147. https://doi.org/10.1016/j.heares.2017.01.003.
López-López, D., Gómez-Nieto, R., Herrero-Turrión, M.J., García-Cairasco, N., Sánchez-Benito, D., Ludeña, M.D., López, D.E., 2017. Overexpression of the immediate-early genes Egr1, Egr2, and Egr3 in two strains of rodents susceptible to audiogenic seizures. Epilepsy Behav. 71 (Pt B), 226–237. https://doi.org/10.1016/j.yebeh.2015.12.020.
Lorente de Nó, R., 1981. The Primary Acoustic Nuclei. Raven Press, New York, NY.
Loscher, W., 2011. Critical review of current animal models of seizures and epilepsy used in the discovery and development of new antiepileptic drugs. Seizure 20, 359–368. https://doi.org/10.1038/nn.3934.
Malmierca, M.S., 2003. The structure and physiology of the rat auditory system: an overview. Int. Rev. Neurobiol. 56, 147–211. https://doi.org/10.1016/S0074-7742(03)56005-6.
Milloy, V., Fournier, P., Benoit, D., Noreña, A., Koravand, A., 2017. Auditory brainstem responses in tinnitus: a review of who, how, and what? Front. Aging Neurosci. 9, 237. https://doi.org/10.3389/fnagi.2017.00237.
Misawa, H., Sherr, E.H., Lee, D.J., Chetkovich, D.M., Tan, A., Schreiner, C.E., Bredt, D.S., 2002. Identification of a monogenic locus (jams1) causing juvenile audiogenic seizures in mice. J. Neurosci. 22 (23), 10088–10093. https://doi.org/10.1523/JNEUROSCI.22-23-10088.2002.
Miyazaki, T., Fukaya, M., Shimizu, H., Watanabe, M., 2003. Subtype switching of vesicular glutamate transporters at parallel fibre-Purkinje cell synapses in developing mouse cerebellum. Eur. J. Neurosci. 17 (12), 2563–2572. https://doi.org/10.1046/j.1460-9568.2003.02698.x.
Mulders, W.H., Ding, D., Salvi, R., Robertson, D., 2011. Relationship between auditory thresholds, central spontaneous activity, and hair cell loss after acoustic trauma. J. Comp. Neurol. 519 (13), 2637–2647. https://doi.org/10.1002/cne.22644.
Muñoz, L.J., Carballosa-Gautam, M.M., Yanowsky, K., García-Atarés, N., López, D.E., 2017. The genetic audiogenic seizure hamster from Salamanca: the GASH:Sal. Epilepsy Behav. 71 (Pt B), 181–192. https://doi.org/10.1016/j.yebeh.2016.03.002.
Nadol Jr., J.B., 1988. Quantification of human spiral ganglion cells by serial section reconstruction and segmental density estimates. Am. J. Otolaryngol. 9 (2), 47–51. https://doi.org/10.1016/s0196-0709(88)80007-3.
Narayanan, P., Chatterton, P., Ikeda, A., Ikeda, S., Corey, D.P., Ervasti, J.M., Perrin, B.J., 2015. Length regulation of mechanosensitive stereocilia depends on very slow actin dynamics and filament-severing proteins. Nat. Commun. 6, 6855. https://doi.org/10.1038/ncomms7855.
N'Gouemo, P., Faingold, C.L., Morad, M., 2009. Calcium channel dysfunction in inferior colliculus neurons of the genetically epilepsy-prone rat. Neuropharmacology 56 (3), 65–75. https://doi.org/10.1016/j.neuropharm.2008.11.005.
Nakashima, M., Takano, K., Osaka, H., Aida, N., Tsurusaki, Y., Miyake, N., Saitsu, H., Matsumoto, N., 2014. Causative novel PNKP mutations and concomitant PCDH15 mutations in a patient with microcephaly with early-onset seizures and developmental delay syndrome and hearing loss. J. Hum. Genet. 59 (8), 471–474. https://doi.org/10.1038/jhg.2014.51.
Nordmann, A.S., Bohne, B.A., Harding, G.W., 2000. Histopathological differences between temporary and permanent threshold shift. Hear. Res. 139 (1–2), 13–30. https://doi.org/10.1016/s0378-5955(99)00163-X.
Oliver, D.L., Ostapoff, E.M., Beckius, G.E., 1999. Direct innervation of identified tectothalamic neurons in the inferior colliculus by axons from the cochlear nucleus. Neuroscience 93 (2), 643–658. https://doi.org/10.1016/s0306-4522(99)00143-8.
Patuzzi, R., 2011. Ion flow in stria vascularis and the production and regulation of cochlear endolymph and the endolymphatic potential. Hear. Res. 277, 4–19. https://doi.org/10.1016/j.heares.2011.01.010.
Penny, J.E., Brown, R.D., Hodges, K.B., Kupetz, S.A., Glenn, D.W., Jobe, P.C., 1983. Cochlear morphology of the audiogenic-seizure susceptible (AGS) or genetically epilepsy prone rat (GEPR). Acta Otolaryngol. 95 (1–2), 1–12. https://doi.org/10.3109/00016488309130909, 1983 Jan-Feb.
Pierson, M., Snyder-Keller, A., 1994. Development of frequency-selective domains in inferior colliculus of normal and neonatally noise-exposed rats. Brain Res. 636 (1), 55–67. https://doi.org/10.1016/0006-8993(94)90175-9.
Pinto, H.P.P., Oliveira Lucas, E.L., Carvalho, V.R., Mourão, F.A.G., Guarnieri, L.O., Mendes, E.M.A.M., Medeiros, D.C., Moraes, M.F.D., 2019. Seizure susceptibility corrupts inferior colliculus acoustic integration. Front. Syst. Neurosci. 13, 63. https://doi.org/10.3389/fnsys.2019.00063.
Prieto-Martín, A.I., Aroca-Aguilar, J.D., Sánchez-Sánchez, F., Muñoz, L.J., López, D.E.,

Escribano, J., de Cabo, C., 2017. Molecular and neurochemical substrates of the audiogenic seizure strains: the GASH:Sal model. Epilepsy Behav. 71 (Pt B), 218–225. https://doi.org/10.1016/j.yebeh.2015.05.025.
Pujol, R., Abonnenc, M., 1977. Receptor maturation and synaptogenesis in the golden hamster cochlea. Arch. Oto-Rhino-Laryngol. 217 (1), 1–12. https://doi.org/10.1007/bf00453886.
Rachel, J.D., Kaltenbach, J.A., Janisse, J., 2002. Increases in spontaneous neural activity in the hamster dorsal cochlear nucleus following cisplatin treatment: a possible basis for cisplatin-induced tinnitus. Hear. Res. 164 (1–2), 206–214. https://doi.org/10.1016/s0378-5955(02)00287-3.
Reigel, C.E., Dailey, J.W., Jobe, P.C., 1986. The genetically epilepsy-prone rat: an overview of seizure-prone characteristics and responsiveness to anticonvulsant drugs. Life Sci. 39 (9), 763–767. https://doi.org/10.1016/0024-3205(86)90454-6.
Ross, K.C., Coleman, J.R., 2000. Developmental and genetic audiogenic seizure models: behavior and biological substrates. Neurosci. Biobehav. Rev. 24 (6), 639–653. https://doi.org/10.1016/s0149-7634(00)00029-4 submitted for publication.
Rubio, M.E., 2019. Molecular and structural changes in the cochlear nucleus in response to hearing loss. In: Kandler, Karl (Ed.), The Oxford Handbook of the Auditory Brainstem. https://doi.org/10.1093/oxfordhb/9780190849061.013.7.
Salvi, R.J., Wang, J., Ding, D., 2000. Auditory plasticity and hyperactivity following cochlear damage. Hear. Res. 147 (1–2), 261–274. https://doi.org/10.1016/s0378-5955(00)00136-2, 2000 Sep.
Sánchez-Benito, D., Gómez-Nieto, R., Hernández-Noriega, S., Murashima, A.A.B., de Oliveira, J.A.C., Garcia-Cairasco, N., López, D.E., Hyppolito, M.A., 2017. Morpho-functional alterations in the olivocochlear efferent system of the genetic audiogenic seizure-prone hamster GASH:Sal. Epilepsy Behav. 71 (Pt B), 193–206. https://doi.org/10.1016/j.yebeh.2016.05.040.
Seal, R.P., Akil, O., Yi, E., Weber, C.M., Grant, L., Yoo, J., Clause, A., Kandler, K., Noebels, J.L., Glowatzki, E., Lustig, L.R., Edwards, R.H., 2008. Sensorineural deafness and seizures in mice lacking vesicular glutamate transporter 3. Neuron 57 (2), 263–275. https://doi.org/10.1016/j.neuron.2007.11.032.
Sievers, F., Higgins, D.G., 2018. Clustal Omega for making accurate alignments of many protein sequences. Protein Sci. 27 (1), 135–145. https://doi.org/10.1002/pro.3290.
Simmons, D.D., Manson-Gieseke, L., Hendrix, T.W., Morris, K., Williams, S.J., 1991. Postnatal maturation of spiral ganglion neurons: a horseradish peroxidase study. Hear. Res. 55 (1), 81–91. https://doi.org/10.1016/0378-5955(91)90094-P.
Simmons, D.D., Rogers, M.S., Woody, D., 1994. Acute effects of capsaicin on the postnatal spiral ganglion. Int. J. Dev. Neurosci. 12 (5), 517–525. https://doi.org/10.1016/0736-5748(94)90036-1.
Schaette, R., McAlpine, D., 2011. Tinnitus with a normal audiogram: physiological evidence for hidden hearing loss and computational model. J. Neurosci. 31 (38), 13452–13457. https://doi.org/10.1523/JNEUROSCI.2156-11.2011.
Schuknecht, H.F., Watanuki, K., Takahashi, T., Belal Jr., A.A., Kimura, R.S., Jones, D.D., Ota, C.Y., 1974. Atrophy of the stria vascularis, a common cause for hearing loss. Laryngoscope 84 (10), 1777–1821. https://doi.org/10.1288/00005537-197410000-00012.
Skradski, S.L., Clark, A.M., Jiang, H., White, H.S., Fu, Y.H., Ptacek, L.J., 2001. A novel gene causing a mendelian audiogenic mouse epilepsy. Neuron 31, 537–544. https://doi.org/10.1016/s0896-6273(01)00397-X.
Takamori, S., 2006. VGLUTs: 'exciting' times for glutamatergic research? Neurosci. Res. 55 (4), 343–351. https://doi.org/10.1016/j.neures.2006.04.016.
Takamori, S., Rhee, J.S., Rosenmund, C., Jahn, R., 2001. Identification of differentiation-associated brain-specific phosphate transporter as a second vesicular glutamate transporter (VGLUT2). J. Neurosci. 21 (22), RC182. https://doi.org/10.1523/JNEUROSCI.21-22-j0002.2001.
Vogler, D.P., Robertson, D., Mulders, W.H., 2011. Hyperactivity in the ventral cochlear nucleus after cochlear trauma. J. Neurosci. 31 (18), 6639–6645. https://doi.org/10.1523/JNEUROSCI.6538-10.2011.
Wallén-Mackenzie, A., Wootz, H., Englund, H., 2010. Genetic inactivation of the vesicular glutamate transporter 2 (VGLUT2) in the mouse: what have we learnt about functional glutamatergic neurotransmission? Ups. J. Med. Sci. 115 (1), 11–20. https://doi.org/10.3109/03009730903572073.
Warr, W.B., Beck, J.E., 1996. Multiple projections from the ventral nucleus of the trapezoid body in the rat, vol. 93, pp. 83–101. https://doi.org/10.1016/0378-5955(95)00198-0 (1–2).
Werner, F.M., Coveñas, R., 2017. Classical neurotransmitters and neuropeptides involved in generalized epilepsy in a multi-neurotransmitter system: how to improve the antiepileptic effect? Epilepsy Behav. 71 (Pt B), 124–129. https://doi.org/10.1016/j.yebeh.2015.01.038.
Xia, A., Song, Y., Wang, R., Gao, S.S., Clifton, W., Raphael, P., Chao, S.I., Pereira, F.A., Groves, A.K., Oghalai, J.S., 2013. Prestin regulation and function in residual outer hair cells after noise-induced hearing loss. PLoS One 8 (12), e82602. https://doi.org/10.1371/journal.pone.0082602.
Yasuda, S., Ishida, N., Higashiyama, A., Morinobu, S., Kato, N., 2000. Characterization of audiogenic-like seizures in naive rats evoked by activation of AMPA and NMDA receptors in the inferior colliculus. Exp. Neurol. 164 (2), 396–406. https://doi.org/10.1006/exnr.2000.7401.
Zeng, C., Nannapaneni, N., Zhou, J., Hughes, L.F., Shore, S., 2009. Cochlear damage changes the distribution of vesicular glutamate transporters associated with auditory and nonauditory inputs to the cochlear nucleus. J. Neurosci. 29 (13), 4210–4217. https://doi.org/10.1523/JNEUROSCI.0208-09.2009.
Zhou, J., Nannapaneni, N., Shore, S., 2007. Vessicular glutamate transporters 1 and 2 are differentially associated with auditory nerve and spinal trigeminal inputs to the cochlear nucleus. J. Comp. Neurol. 500 (4), 777–787. https://doi.org/10.1002/cne.21208.